



I&C for the CIET 1.0 Facility

**Instrumentation and Controls Development for the Compact Integral
Effects Test Facility**

Thermal Hydraulics Laboratory

Author

Rohit Upadhyia

Reviewer

James Kendrick

UCBTH-15-006
Revision 2

12 September 2015

Department of Nuclear Engineering
University of California, Berkeley



Executive Summary

Fluoride-salt-cooled, high temperature reactors (FHRs) are a next-generation nuclear power plant concept that utilizes molten fluoride salts as the coolant. The use of molten salts allows the reactor to operate at low pressures—which removes the need for thick concrete containment domes—and allows for high operational temperatures and power densities. In addition, FHRs are highly suitable for the implementation of passive decay heat removal systems, bringing inherent safety to the design.

In order for any reactor design to enter into commercial production, the design must first be licensed by the Nuclear Regulatory Commission, which requires all technical aspects of the reactor's design to be validated with both computational and experimental data. For this purpose, a scaled non-nuclear heat transfer facility has been constructed at University of California, Berkeley, in order to validate thermal hydraulic codes that predict the integral steady-state and transient performance of FHRs. The facility was constructed with funds from an Integrated Research Project (IRP) created by the Department of Energy (DoE), that is also funding FHR-related projects at University of Wisconsin—Madison and the Massachusetts Institute of Technology.

UC Berkeley's facility, the Compact Integral Effects Test Facility (CIET), is a two-loop heat transfer system uses a simulant fluid in place of fluoride salt. The simulant fluid, Dowtherm A, was selected based on scaling analysis that matched key heat transfer and fluid dynamic parameters in a full-scale FHR for smaller length scales and at lower temperatures and flow velocities. CIET is able to model an FHR's primary loop and the Direct Reactor Auxiliary Cooling System (DRACS) loop, which is the natural circulation loop that can passively remove decay heat from the reactor. Other important sections of CIET include the Coiled-Tube Air Heater (CTAH), which models the heat exchanger between the primary loop and power conversion system in a full-scale FHR, and a resistive electrical heater, which models the nuclear core of an FHR.

CIET has gone through a number of initial start-up tests, such as friction-loss analysis, parasitic heat loss characterization, and more advanced tests involving natural circulation and transient responses. During construction, instrumentation and control hardware was installed and configured. In conjunction with testing, feedback control algorithms were developed and optimized for each of the control sub-systems. Various types of control algorithms and tuning strategies were used and compared with one another for the different sub-systems, with focus on the CTAH.

Contents

Executive Summary	2
Contents	3
List of Figures.....	5
List of Tables	8
Acronyms and Abbreviations	9
1 Introduction.....	10
2 Hardware-Software Installation and Integration	12
2.1 Instrumentation Installation and Integration.....	13
2.1.1 Thermocouples	13
2.1.2 Flow Meters.....	15
2.1.3 Data Acquisition System	18
2.2 Controller Installation and Integration.....	20
2.2.1 Power Supplies	20
2.2.2 Variable Frequency Drives.....	22
3 Feedback Control Theory	27
3.1 Trial-and-Error Tuning.....	28
3.2 Ziegler-Nichols Tuning	28
3.3 Relay Feedback.....	29
3.4 Process Reaction Curves for Model Construction	30
3.5 Internal Model Tuning	31
3.6 ITAE-1.....	31
4 Application and Results for CIET Controllers	32
4.1 Power Supplies	32
4.2 Pump.....	33
4.3 CTAH	37

CIET 1.0 I&C REPORT

4.3.1	Manual Tuning	37
4.3.2	Process Reaction Curve, Model Construction, and Model-Based Tuning	43
4.3.3	Relay Feedback Tuning	46
4.3.4	Summary of Results and Recommendations	49
4.4	TCHX	50
4.4.1	Relay Feedback Tuning	50
5	LabVIEW Code Overview	53
5.1	Instrumentation Data Acquisition	53
5.1.1	Thermocouples	54
5.1.2	Flow Meters	55
5.1.3	Alarms	55
5.1.4	Notes on Extra Elements	57
5.2	Variable Frequency Drive	59
5.2.1	Communication	59
5.2.2	Pre-Operation and Normal Operation	60
5.2.3	Emergency Stop Code for the Pump	61
5.3	Power Supply Base	62
5.3.1	Communication and Initialization	62
5.3.2	Voltage/Current Control Code	63
5.4	Feedback Control Algorithm	64
5.5	Relay Feedback	67
6	Summary and Conclusions	69
7	References	70

List of Figures

Figure 1. CIET flow path layout.....	11
Figure 2. Data-flow diagram of CIET instruments and controllers.....	12
Figure 3. Photo of one of CIET's flow meter transmitter.....	17
Figure 4. Flow meter transmitter connection diagram.....	17
Figure 5. Section of the NI MAX window that shows detected devices and interfaces.....	19
Figure 6. "Channel Calibration Properties" Window from the DAQ Assistant.....	20
Figure 7. Wiring diagram of two power supplies in series with a load.....	21
Figure 8. LabVIEW block diagram of the initialization code for the power supplies.....	22
Figure 9. Visual depiction of the GS1 VFD.....	23
Figure 10. NI Measurement and Automation Explorer window, used to configure communication ports.....	24
Figure 11. LabVIEW block diagram of the Modbus Sub-VI used to communicate with the VFDs.....	25
Figure 12. Graph of controller input and process output during relay feedback operation... ..	30
Figure 13. Graphical comparison of open-loop and resistance feedback control strategies for the power supplies.....	33
Figure 14. Pump curve from technical sheet.....	34
Figure 15. Pump response for a set-point change from 0.1 kg/s to 0.18 kg/s, for a range of proportional gain coefficients for an actuation frequency of 2 s.....	35
Figure 16. Pump response for a set-point change from 0.18 kg/s to 0.1 kg/s, for a range of proportional gain coefficients for an actuation frequency of 2 s.....	36
Figure 17. Pump response for a set-point change from 0.1 kg/s to 0.18 kg/s, for a range of actuation frequencies for a proportional gain of 730.....	37
Figure 18. CTAH outlet temperature response for a proportional controller with a gain of 10 and an actuation frequency of 20 s, during a heat-up and power step-change scenario.....	38
Figure 19. CTAH outlet temperature response of two controllers. The actuation frequency was 20 s for the set-point of 75°C, and 10 s for the set-point of 70°C.....	39
Figure 20. CTAH outlet temperature response to a step-change in the mass flow-rate, for a P-Controller with a proportional gain of 10 and an actuation timer of 10 s.....	40

Figure 21. CTAH outlet temperature response to a step-change in the mass flow-rate from 0.10 kg/s to 0.08 kg/s, for a P-controller with a proportional gain of 10 and an actuation timer of 30 s. 40

Figure 22. CTAH outlet temperature response to a step-change in the mass flow-rate from 0.08 kg/s to 0.05 kg/s, for a PD-Controller with a proportional gain of 3, a derivative gain of 100, and an actuation frequency of 30 s. 41

Figure 23. Comparison of the CTAH outlet temperature response when controlled by a P and a PD controller, each with an actuation frequency of 30 s. 41

Figure 24. CTAH outlet temperature and motor responses for two different actuation frequencies, given a proportional gain of 10 and an outlet temperature set-point of 80 C..... 42

Figure 25. CTAH temperature response to power step-changes, with the outlet temperature controlled with a P-Controller with proportional gain of 10 and an actuation frequency of 15 s. 43

Figure 26. CTAH motor response to power step-changes, with aforementioned conditions. 43

Figure 27. PRC test at normal, steady-state conditions with a frequency step-change of +5.0 Hz..... 44

Figure 28. Comparison of IMC and ITAE-1 PID controllers during CIET start-up. 46

Figure 29. Relay feedback test for CTAH at normal, steady-state conditions and relay amplitudes of 2.0 and 2.5 Hz. 47

Figure 30. Comparison of a standard PID controller and a no-overshoot PID controller, derived from relay feedback testing, during CIET start-up. 48

Figure 31. Comparison of the CTAH outlet temperature response when controlled by a standard PID controller and a no-overshoot PID controller. 49

Figure 32. Comparison of a manually-tuned P controller and a relay feedback tuned PID controller during CIET start-up. 50

Figure 33. Relay feedback test for TCHX at power input at 2 kW with coupled natural circulation between the primary and DRACS loop, for relay amplitudes of 2.0, 3.0, and 1.0 Hz. 51

Figure 34. Comparison of a standard PID controller and a no-overshoot PID controller for the TCHX, derived from relay feedback testing. 52

Figure 35. DAQ Assistant block..... 53

Figure 36. Splitting and combing the DAQ Assistant's data output wire. 54

Figure 37. Final signal splitting and data conversion for heater thermocouples. 55

Figure 38. Final signal splitting, data conversion, and current-to-mass-flow conversion for flow meters..... 55

Figure 39. Temperature alarms for fluid and surface temperatures. 56

Figure 40. Alarm sub-VI code with array functions for finding the temperature extrema. 57

Figure 41. Error calculation for the Pump Mass Flow Rate. 57

Figure 42. Error calculation for the CTAH Outlet Temperature. 58

Figure 43. Example of bundling data measurements. 58

Figure 44. Graphing loop. 58

Figure 45. Section of a front panel for controlling the VFDs for the pump and fans. 59

Figure 46. Inputs and outputs to the CTAH VFD's Modbus sub-VI. 60

Figure 47. A counting algorithm to cycle the GS1 Set-Up sub-VI through the relevant sets of addresses and holding registers to prepare the VFDs for running. 60

Figure 48. GS1 Set-Up sub-VI code for setting key parameters. 61

Figure 49. Normal control mode for the CTAH VFD. 61

Figure 50. Pump VFD frequency coercion code and primary loop mass flow rate monitor. 61

Figure 51. Front panel for power supply control. 62

Figure 52. Initialization code for the power supplies. 63

Figure 53. Series of sub-VIs for controlling and monitoring one power supply. 63

Figure 54. Section of power control code that coverts the Desired Power into the voltage limit. 64

Figure 55. Processing the resistance calculation prior to transferring it to the next loop iteration. 64

Figure 56. Proportional controller for the pump. 65

Figure 57. The CTAH PID feedback control algorithm. 66

Figure 58. Integrator loop. 66

Figure 59. Differentiator loop. 67

Figure 60. Relay Feedback Loop for tuning the CTAH. 67

Figure 61. Noise gate code for optimal relay feedback performance. 68

List of Tables

Table 2-1. List of thermocouples in the different sections of CIET.	14
Table 2-2. Table of thermocouples, module and channel assignments, and physical location in CIET.	15
Table 3. Technical requirements for the flow meters.	16
Table 2-4. List of communication parameters that must be set prior to remote control of the VFDs.	23
Table 2-5. Table of motor-dependent parameters that must be set before the VFD can properly control the motors.	25
Table 3-1. List of Ziegler-Nichols tuning rules, based on the ultimate gain and ultimate period.	29
Table 4-1. Results of PRC testing on CTAH at normal, steady-state conditions.	45
Table 4-2. Theoretically optimal PID coefficients based on FOTD-based tuning rules.	45
Table 4-3. PID coefficients derived from FOTD model-based tuning rules that were selected for testing.	45
Table 4-4. PID coefficients for CTAH control derived from the relay feedback test.	47
Table 4-5. PID coefficients for CTAH control derived from the relay feedback test.	51

Acronyms and Abbreviations

CIET – Compact Integral Effects Test
CTAH – Coiled Tube Air Heater
DAQ – Data Acquisition
DHX – DRACS Heat Exchanger
DRACS – Direct Reactor Auxiliary Cooling System
FHR – Fluoride-Salt-Cooled High-Temperature Reactor
FOTD – First Order plus Time Delay
GPM – Gallons per Minute
IMC – Internal Model Control
ITAE-1 – Integral of the Time-Weighted Absolute value of the Error for a First Order Time Delay model
LUI – Local User Interface
MAX – Measurement and Automation Explorer
RPM – Rotations per Minute
NI – National Instruments
P – Proportional
PB-FHR – Pebble-Bed Fluoride-Salt-Cooled High-Temperature Reactor
PI – Proportional-Integral
PID – Proportional-Integral-Derivative
PD – Proportional-Derivative
PRC – Process Reaction Curve
TCHX – Thermosyphon-Cooled Heat Exchanger
UCB – University of California, Berkeley
VFD – Variable Frequency Drive
VISA – Virtual Instrument Software Architecture
ZN – Ziegler-Nichols

1 Introduction

The Fluoride-Salt-Cooled High-Temperature Reactor (FHR) is a Generation IV nuclear reactor concept. FHRs use molten salts as the primary coolant, which enables them to have benefits over conventional water-cooled reactors. Fluoride salts have very high boiling points (often over 1400°C), allowing FHRs to operate at high temperatures, which maximize thermal efficiency, and low pressures, which minimize costs associated with pressure vessels and concrete containment domes. The thermophysical properties of molten salt also enable FHRs to be designed with passive safety systems, minimizing dependence on human intervention during emergency events and accident scenarios.

A key step in the licensing process for next-generation nuclear reactors is to validate the effectiveness of thermal hydraulics codes in predicting the reactor performance. Typically, code validation is done by comparing the code predictions to actual dynamics observed in an integral test facility. University of California, Berkeley (UCB) has designed and constructed the Compact Integral Effects Test (CIET) Facility, a scaled facility that simulates the steady-state and transient thermal hydraulic response of FHRs under forced and natural circulation modes. The facility is based on scaling methodologies developed specifically for the development of FHRs (Bardet and Peterson 2007). CIET uses Dowtherm A, an organic heat transfer fluid that is able to match the Prandtl, Reynolds, Grashof, and Froude dimensionless numbers of molten fluoride salts with minimal distortion. The prototype design that CIET simulates, at 50% geometry and 2% power scales, is the 900 MWth Pebble-Bed Advanced High-Temperature Reactor (Bardet et al. 2008). CIET is also able to match the dynamics of a more recent prototype design, the 236 MWth Mark I Pebble-Bed FHR (PB-FHR) with small distortion (Andreades et al. 2014).

CIET has two fluid loops, a primary and a Direct Reactor Auxiliary Cooling System (DRACS) loop. The primary loop contains four legs: one leg for the heat source, two legs for heat exchangers, and one bypass leg. CIET uses a resistive heater powered with two electrical power supplies to model the FHR's nuclear core. The Coiled-Tube Air Heater (CTAH) models heat exchange in the FHR from the primary loop to the power conversion system; this is a key part of normal operation. The DRACS Heat Exchanger (DHX) models heat exchange in the FHR from the primary loop to the DRACS loop; this is a key part of an FHR's emergency response mode for decay heat removal. Heat is transferred out of the DRACS loop via the Thermosyphon-Cooled Heat Exchanger (TCHX). The primary loop can operate in both forced and natural circulation, while the DRACS loop can only operate in natural circulation. Figure 1 shows a diagram of CIET's layout.

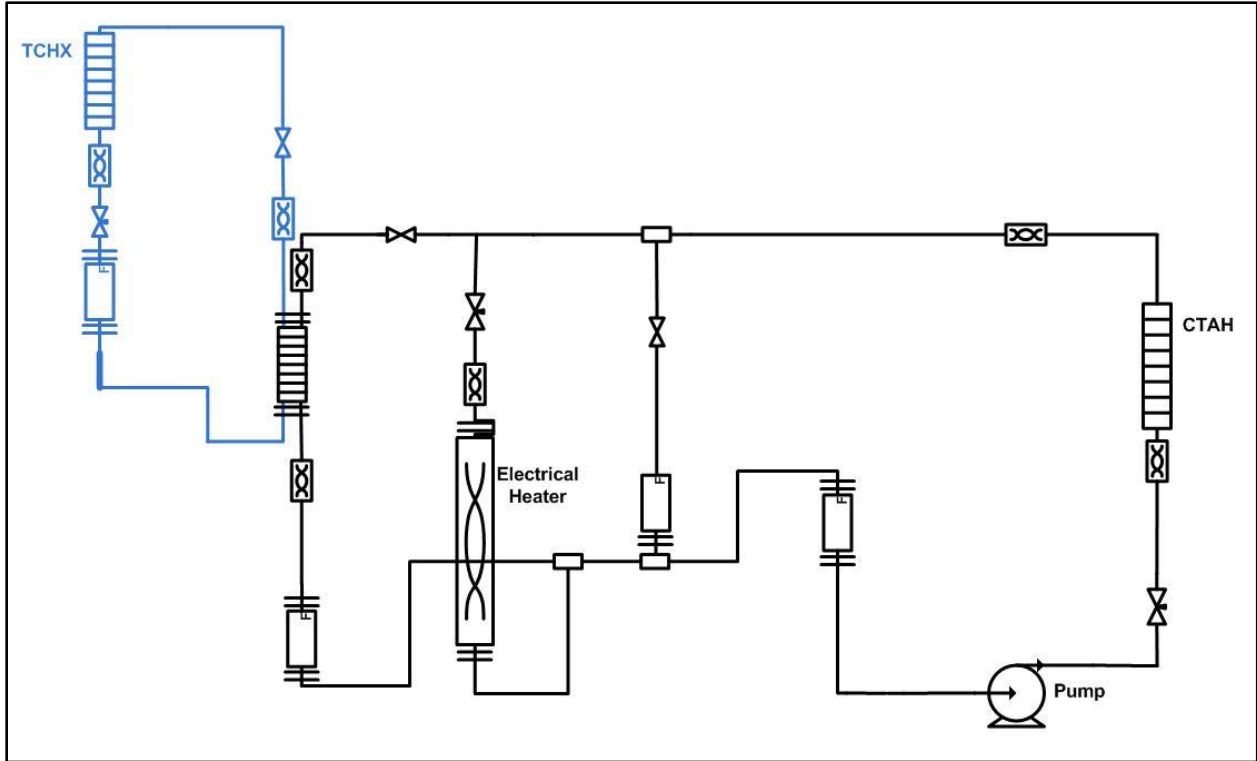


Figure 1. CIET flow path layout

In order for CIET to be fully functional, all instrumentation and control systems must be properly connected and integrated with the proper physical and virtual systems. Instrumentation measures key parameters such as temperature, pressure, flow rates, etc. that are critical for both effective and safe operation of CIET, as well as for data collection and analysis purposes. Section 2 discusses the instrumentation and control hardware, as well as the underlying software used to tie the hardware together. This section also focuses on installation and integration guidelines and procedures for thermocouples, flow meters, power supplies, and variable frequency drives.

Controller development and optimization is necessary to ensure that CIET is able to operate smoothly and safely, and to ensure that the observed dynamics actually reflect FHR dynamics consistently. There are a variety of different theories around controls engineering and optimization strategies, and much of the controls work on CIET involved applying different theories and methods to the individual control sub-systems. Section 3 discusses the theory behind various feedback control development methodologies, and Section 4 discusses the application of these methodologies to CIET, and compares the performance of various controllers and methodologies for the different components. LabVIEW is used to integrate all of CIET's instrumentation and controller systems together into a central communication, control, and data-processing system. The LabVIEW code developed and used for CIET's feedback control development and optimization is discussed in Section 5.

2 Hardware-Software Installation and Integration

The building blocks of CIET’s control systems lie in the hardware and software, in the form of the various instruments and controllers used to collect data and manipulate processes and the software used to process signals and manipulate controllers. A computer functions as the central processor that takes in data inputs and outputs directions for the controllers. The inputs to the computer are thermocouple and flow meter signals, and the outputs control two power supplies, a pump, and two fan-cooled heat exchangers. Figure 2 shows the data flows of the key instruments and controllers with respect to the computer; note that the power supply (referred to as a singular power supply as the two power supplies are controlled as one unit) is the only component that has both inputs and outputs.

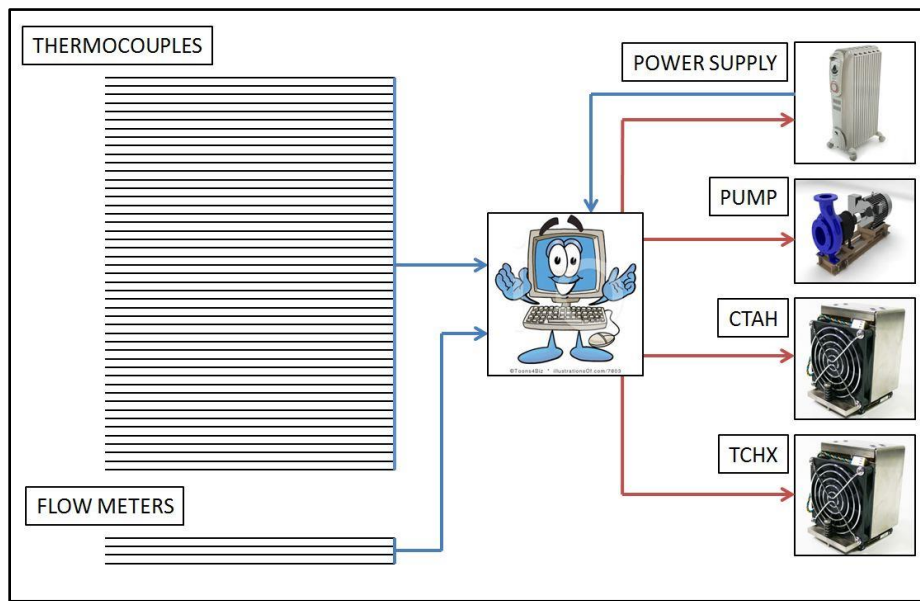


Figure 2. Data-flow diagram of CIET instruments and controllers.

Instrumentation

- National Instruments (NI) Data Acquisition (DAQ) Hardware—Set of hardware that is used to monitor and process measurements from the thermocouples and flow meters, and interface them with computer programs.
 - SCXI-1000 (1)—Chassis for the DAQ hardware, can be outfitted with different modules depending on system needs
 - SCXI-1600 (1)—Module for connecting the DAQ hardware to a PC with a USB cable; transfers data from instruments attached to the DAQ to the computer
 - SCXI-1102B (2)—Thermocouple signal reader module; is inserted into the chassis, and interfaces between the chassis and the attached terminal block; also reads signals from the flow meters

- SCIX-1303 (2)—Thermocouple signal reader terminal block; attaches to the module; has 32 analog input slots (channels) that can convert the thermocouple’s voltage differential into a corresponding temperature value
- Omega Type T Thermocouples (42)—Measures temperatures; attaches into the DAQ thermocouple reader terminal blocks, which can read the thermocouple’s voltage difference
- Conax Thermocouples (8)—Measures temperatures in two locations in CIET (four thermocouples in two locations, measuring temperature at different radial locations in the fluid path)
- Siemens SITRANS FC430 Coriolis Flow Meters (4)—Measures the mass flow rate at the installed location, and is connected to a remote sensor terminal (SCIX-1303); outputs 4 – 20 mA DC signals that can be read by the DAQ system

Controllers

- Supply (2)—A low-voltage, high-current power supply that can operate in constant voltage or constant current mode, with remote control capabilities; provides resistive heating to CIET
- Automation Direct GS1-10P5 Variable Frequency Drive (VFD) (3)—A 1/4 hp VFD converts a single-phase power input into a variable three-phase power output; output frequency can be actuated via computer control
- Price Pump Company HP Centrifugal Pump (1)—Pump with a roughly linear relationship between motor rotational speed and mass flow rate

Software

- National Instruments LabVIEW Full Development System—Graphical programming language with in-built input-output (I/O) modules for measurement and control tasks.
- Origin—Data analysis and graphing program

2.1 Instrumentation Installation and Integration

All the instruments—the thermocouples and the flow meters—ultimately connect into the DAQ system, into one of the two thermocouple signal reader blocks. Due to the large number of wiring, care must be taken to properly plan out wire paths and arrange wires so that they are not putting pressure on one another.

2.1.1 Thermocouples

Thermocouples use the difference in resistance vs. temperature dependencies of two different materials to generate a voltage signal that corresponds to temperature. Thermocouples operate in different temperature ranges depending on the type of material. CIET uses Type T

thermocouples, which use copper and nickel as the sensing materials, and can operate between -250°C to 350°C.¹

Optimal placement of thermocouples depends on what parts of a system a user wants or needs to measure. For CIET, the primary areas of concern are around areas of heat exchange, such as before and after heat exchangers, in and around heaters, etc.

Table 2-1 shows the number of locations at each section of CIET.

Table 2-1. List of thermocouples in the different sections of CIET.

Section of CIET	Number of Thermocouples
Heater Leg	8 Conax, 4 Type T
Heater Surface	5 Type T
Bypass Leg	6 Type T
CTAH Leg	4 Type T
DHX Leg	8 Type T
DRACS Loop	8 Type T
Ambient Air	2 Type T

The thermocouples were divided between the two thermocouple signal reader terminal blocks in order to maximize space, and to increase the chance that hard-to-reach analog inputs in the block would not be needed. Prior to connections, the best input locations were noted and assigned to thermocouples, with a general rule that thermocouples in the same location were grouped next to one another.

The thermocouple signal reader terminal blocks are automatically named “Module 2” and “Module 3” (with “Module 1” being the USB module), and are shortened to “Mod2” and “Mod3”. The channels are numbered from 0 to 31, and are named “ai0”, “ai1”, and so forth through “ai31”. Thus, for a thermocouple attached to the 14th input on the third module, the name would be “Mod3/ai13”. Table 2-2 shows the assigned values for the thermocouples.

¹ “Thermocouples: Introduction to Temperature Measurement”. *Omega*. 2015. <http://www.omega.com/prodinfo/thermocouples.html>

Table 2-2. Table of thermocouples, module and channel assignments, and physical location in CIET.

Physical Location	TC	Mod/Channel	Physical Location	TC	Mod/Channel	
Heater Leg	CX-10	Mod2/ai1	DRACS Loop	BT-60	Mod3/ai0	
		Mod2/ai2		WT-61	Mod3/ai1	
		Mod2/ai3		WT-62	Mod3/ai2	
		Mod2/ai4		BT-63	Mod3/ai3	
	CX-11	Mod2/ai5		WT-64	Mod3/ai4	
		Mod2/ai6		BT-65	Mod3/ai5	
		Mod2/ai7		BT-66	Mod3/ai6	
		Mod2/ai8		WT-67	Mod3/ai7	
	WT-10	Mod2/ai10		DHX Leg	WT-20	Mod3/ai20
	BT-11	Mod2/ai11			BT-21	Mod3/ai21
BT-12	Mod2/ai12	WT-22	Mod3/ai22			
WT-13	Mod2/ai13	BT-23	Mod3/ai23			
Bypass Leg	BT-30	Mod2/ai20	WT-24		Mod3/ai24	
	WT-31	Mod2/ai21	BT-25	Mod3/ai25		
	BT-32	Mod2/ai22	WT-26	Mod3/ai26		
	WT-33	Mod2/ai23	BT-27	Mod3/ai27		
	BT-34	Mod2/ai24	WT-28	Mod3/ai28		
	WT-35	Mod2/ai25	BT-29	Mod3/ai29		
CTAH Leg	WT-40	Mod2/ai27	Heater Surface	ST-10	Mod3/ai10	
	BT-41	Mod2/ai28		ST-11	Mod3/ai11	
	WT-42	Mod2/ai29		ST-12	Mod3/ai12	
	BT-43	Mod2/ai30		ST-13	Mod3/ai13	
			ST-14	Mod3/ai14		
		Ambient Air	AT-01	Mod3/ai30		
			AT-02	Mod3/ai31		

The thermocouple readings can be read through LabVIEW through the DAQmx software, which will be specified in Section 2.2.3.

2.1.2 Flow Meters

Four Siemens SITRANS FC430 Coriolis Flow Meters are used to measure mass flow rates in CIET. There are three flow meters in the primary loop, measuring flow rates in the CTAH, bypass, and DHX legs, and one flow meter in the DRACS loop. The entire set-up consists of a flow meter in the corresponding location in the system, a transmitter interface that controls and measures the physical flow meter, and cables that communicate between the flow meter and the

transmitter, and the transmitter and the DAQ. Table 3 shows technical requirements and specifications of each flow meter, with a complete table found in the flow meter technical sheet.²

Table 3. Technical requirements for the flow meters.

Flow Meter	FM-20	FM-30	FM-40	FM-60
Location	DHX	Bypass	CTAH	DRACS
Sensor	FCS400 DN25	FCS400 DN15	FCS400 DN25	FCS400 DN25
Maximum Flow Rate [kg/h]	88,400	31,900	88,400	88,400
Connections	ANSI B16.5 class 150, 1" flange	ANSI B16.5, class 150, 3/4" flange w/ reducer	ANSI B16.5 class 150, 1" flange	ANSI B16.5 class 150, 1" flange

The flow meters connect to the transmitters with four-wire cables with M12 connectors, which are supplied by the vendor. The transmitters communicate to the DAQ using 4-20 mA HART cables. These are connected into the thermocouple sensor modules on the DAQ. Because the modules are voltage sensors primarily used for thermocouples, resistors need to be added into the module so that the current is converted into a voltage signal. There are three I/O channels for the transmitter; CIET uses Channel 1. The transmitters need to be connected to a source of power, 100-240 V AC power with 47-63 Hz. Figure 3 and Figure 4 show a photo and a diagram of the flow meter transmitter connections.

² Zweibaum, Nicholas. *SITRANS FC430 Coriolis Flowmeters Technical Sheet*. CIET-MES-TS-002-01. Thermal Hydraulics Group. 2014.



Figure 3. Photo of one of CIET's flow meter transmitter.

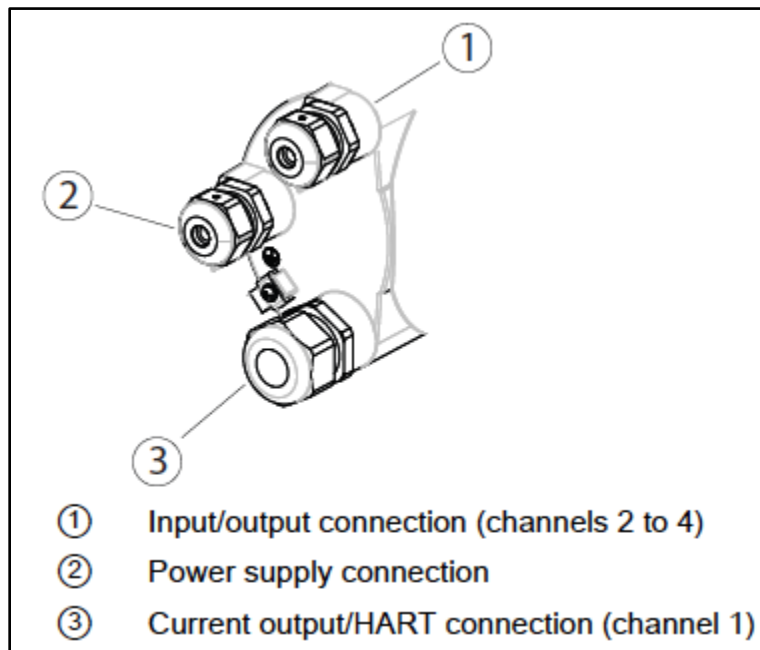


Figure 4. Flow meter transmitter connection diagram.

The flow meters must be configured via the transmitter’s Local User Interface (LUI) prior to operation. The general navigation method for the LUI is to use the right arrow to select an option (or, from the default measurement display window, to access the menus), and the left arrow to go back to the previous window. The up and down arrows are used to navigate up and down the menus.

There are three access levels for the transmitter, for security and access control purposes. The “Read Only” access level allows a user to view the settings, but does not allow changes. The “User” access level allows a user to change all parameters except for calibration parameters;

the default PIN for this access level is 2457. The “Expert” access level is the highest access level, and allows all parameters—including calibration parameters—to be modified. The default PIN for this access level is 2834.

There are a number of parameters that must be configured prior to first operating the flow meters in CIET. Some are specific to only certain flow meters.

The following parameters are applied to all the flow meters, and can be found under the “Quick Start” menu:

- Flow Direction: Positive
- Mass Flow: Unit: kg/s, Low Flow Cut-Off: 0.00 kg/s
- Volume Flow: Unit: m³/s, Low Flow Cut-Off: 0.00 m³/s
- Density: Unit: kg/m³
- Fluid Temperature: Unit: °C

The alarm, warning, and current output parameters are specific to certain flow meters, and can be found under the “Setup” menu.

The alarms and warnings for the mass flow can be found by navigating into “Process Values: Massflow”. The required settings are:

- Upper Limit Alarm: 0.50 kg/s
- Upper Limit Warning: 0.50 kg/s
- Lower Limit Warning: -0.50 kg/s (FM-20, FM-40); -0.10 kg/s (FM-30, FM-60)
- Lower Limit Alarm: -0.50 kg/s (FM-20, FM-40); -0.10 kg/s (FM-30, FM-60)

The current output settings can be found by navigating into “Inputs/Outputs: Current Output”. The required settings are:

- Process Value: Massflow
- Direction: Bidirectional (FM-20, FM-40); Positive (FM-30, FM-60)
- Upper Scaling: 0.50 kg/s
- Lower Scaling: -0.50 kg/s (FM-20, FM-40); 0.00 kg/s (FM-30, FM-60)

The settings for the Zero-Point Adjustment can be found by navigating into “Zero Point Adjustment”. The required settings are:

- Duration: 60 s
- Standard Deviation Limit: 0.01 kg/s

2.1.3 Data Acquisition System

In order to read the measurements from the instruments connected to the DAQ, a DAQ Assistant Sub-VI must be configured in a LabVIEW VI. The DAQ Assistant is available after download and installation of the NI-DAQmx drivers. The NI Measurement and Automation Explorer (MAX) can be used to confirm that the PC has detected the DAQ system and the associated modules, by clicking in the left-hand window through the *Devices and Interfaces*; the attached SCXI systems should show up, as shown in Figure 5.

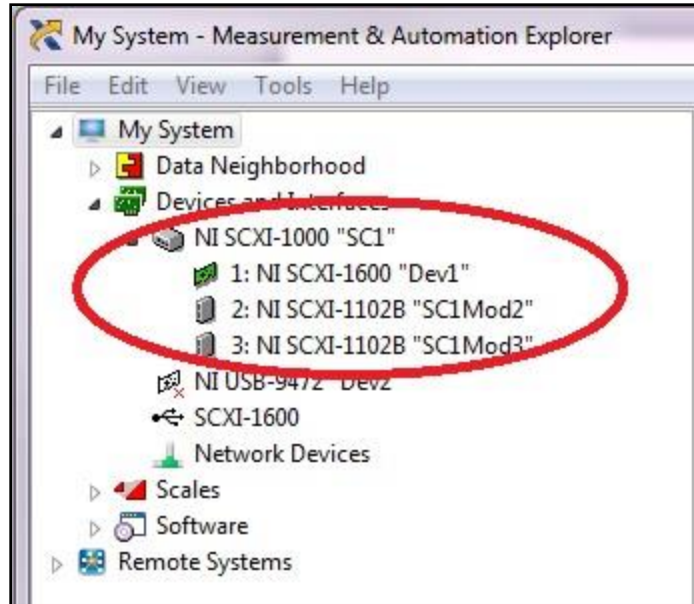


Figure 5. Section of the NI MAX window that shows detected devices and interfaces.

The DAQ Assistant can be found in the Functions palette for programming in the LabVIEW block diagram, under *Express*>>*Input*. When first creating the program, creating a new DAQ Assistant block will open a “Create New...” window to configure the DAQ. For CIET, the selected measurement type is “Thermocouple”, which is found under *Acquire Signals*>>*Analog Input*>>*Temperature*. Once one channel is selected, the “Create New...” window will close and the primary DAQ Assistant window will open up, where more channels can be added, and channels can be named, calibrated, and customized for specific types of instruments. The DAQ Assistant window can also be used to read the instrument signals, without having to run the main VI.

Instruments can be calibrated by clicking on the “Calibration” Tab, and then the “Properties” button. A window (shown in Figure 6) will appear, and under the “Values” tab the calibration data can be seen. These can be manually modified, or calibrated in real time, by clicking on the relevant button on the right-hand side of the window to access a specific option.

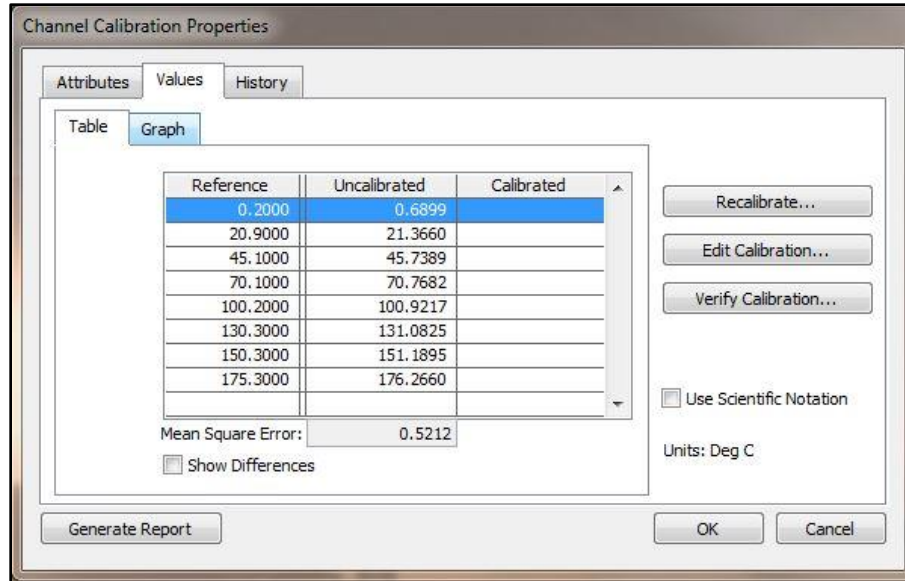


Figure 6. "Channel Calibration Properties" Window from the DAQ Assistant.

2.2 Controller Installation and Integration

The controllers for CIET consist of two power supplies and three VFDs. All controllers have remote-control capabilities that allow them to be subject to feedback control algorithms and automation scripts. Communication takes place through common industrial communication protocols such as Virtual Instrument Software Architecture (VISA) and Modbus.

2.2.1 Power Supplies

There are two aspects to installing the power supplies and integrating them into the rest of the system: 1) installing input AC power and connecting the power supplies to the heater, and 2) setting up remote communication from the PC. Much of this information can be found in the technical manual for the power supplies.³

The power supplies take in an input of 208V, 60Hz AC power. The input power line is 4-wire (3 power + 1 ground).

The two power supplies were connected in series with the heater and with each other using four 4/0 AWG wires. In addition, two copper wires were attached between the load and the sensor inputs of the power supply: these wires are for remote sensing mode, which means that the power supplies read the voltage across the load, rather than at the immediate output node of

³ *Technical Manual for Genesys 10kW/15kW Programmable DC Power Supplies.* TDK-Lambda Americas Inc. 2008.

the power supplies. These wires were twisted with one another to reduce noise. Figure 7 shows the wiring diagram of the power supplies in series with the heater.

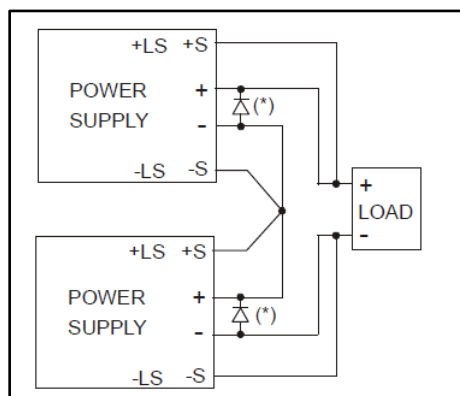


Figure 7. Wiring diagram of two power supplies in series with a load.

The communication wires are also arranged in series. The computer connects to one power supply via an Ethernet cable with a USB-RJ45 adapter, then that power supply is connected to the other one with an RS485 cable. Once connected, the power supplies should show up as a detected device attached to a serial port.

In order to be able to control the power supplies from the computer, several settings need to be set manually:

- Remote mode needs to be set by pressing the REM/LOC button and ensuring that the REM LED is on
- The addresses of the power supplies must be set by holding down the REM/LOC button for around three seconds, and then adjusting the address with the VOLTAGE knob (address options are between 0 and 30); on CIET, the power supplies were addressed as 1 and 2
- The baud rate (communication speed) must be set by holding down the REM/LOC button for around three seconds, and then adjusting the baud rate with the CURRENT knob; on CIET, the baud rate was 9600
- The SW1 switch (on the rear panel) must be in the upward position to ensure that remote control is enabled

Once the power supplies' address and baud rate are set, and the communication wires are hooked up, they can be controlled remotely from the computer through LabVIEW. A screenshot of the LabVIEW code can be seen in Figure 8.

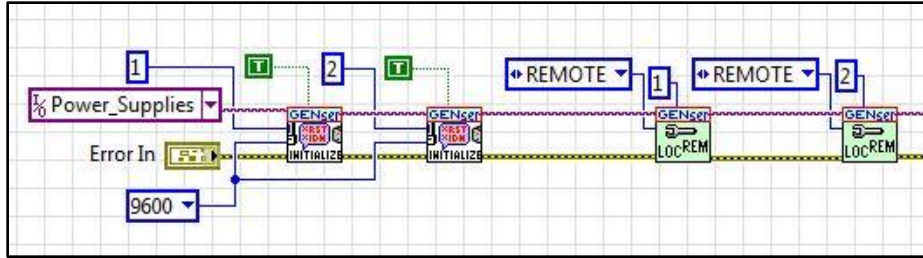


Figure 8. LabVIEW block diagram of the initialization code for the power supplies.

See Section 5.3 for more details on programming and manipulating the power supplies through LabVIEW.

2.2.2 Variable Frequency Drives

VFDs are used to control motors by actuating the output frequency, which has a linear relationship with the motor's rotations per minute (RPM). On CIET, three VFDs are used to control the pump, the CTAH, and the TCHX. The GS1 10P5 takes in a single-phase 100-120V power (wall power) and outputs three-phase AC power. 12-16 AWG copper wire is used to connect the power output from the wall into the VFDs, and from the VFDs to the motors on the pump and the fans. Figure 9 shows a visual depiction of the front face of the VFD. The T terminals at the bottom are for the input power, and the L terminals at the top are for the output power.



Figure 9. Visual depiction of the GS1 VFD.⁴

Communication between the VFD and the computer is done through a USB-485M cable, which converts a RJ12 cable that plugs into the VFD into a USB that plugs into the computer. When connected, the computer will acknowledge that a device is plugged into a serial port. Multiple VFDs can be controlled with one USB port, by plugging in the different RJ12 cables into a telephone splitter, which then connects into the USB-485M converter.

In order to be able to control the power supplies from the computer, several settings need to be set manually. Settings are changed by pressing the “PROG/ENTER” button and using the up and down arrow buttons to navigate through the different parameters. Table 2-4 shows the critical parameters and the values used.

Table 2-4. List of communication parameters that must be set prior to remote control of the VFDs.

Parameter	Value	Description
P3.00	03	Enables RS-485 communication
P4.00	05	Enables RS-485 control of frequency
P9.00	01, 02, or 03	Sets address

⁴ GS1 Series Drives User Manual. Automation Direct. 2nd Edition. July, 2011.

CIET 1.0 I&C REPORT

P9.01	01	Sets baud rate to 9600
P9.02	05	Sets communication protocol to Modbus RTU, 8 bits, odd parity, 1 stop bit

In order to communicate to the VFDs through the computer, the addresses and communication rate in the computer must be set to be the same as the VFDs. This can be accomplished through NI MAX, which can be seen in Figure 10. The serial port that the VFDs are connected to can be found at the left of the NI MAX window, by clicking through *Devices and Interfaces* >> *Serial & Parallel*. In the middle window, there is a tab at the bottom that selects between two options: *General* and *Port Settings*. Under *Port Settings*, the baud rate, data bits, parity, and stop bits can be modified to match the setting on the VFDs.

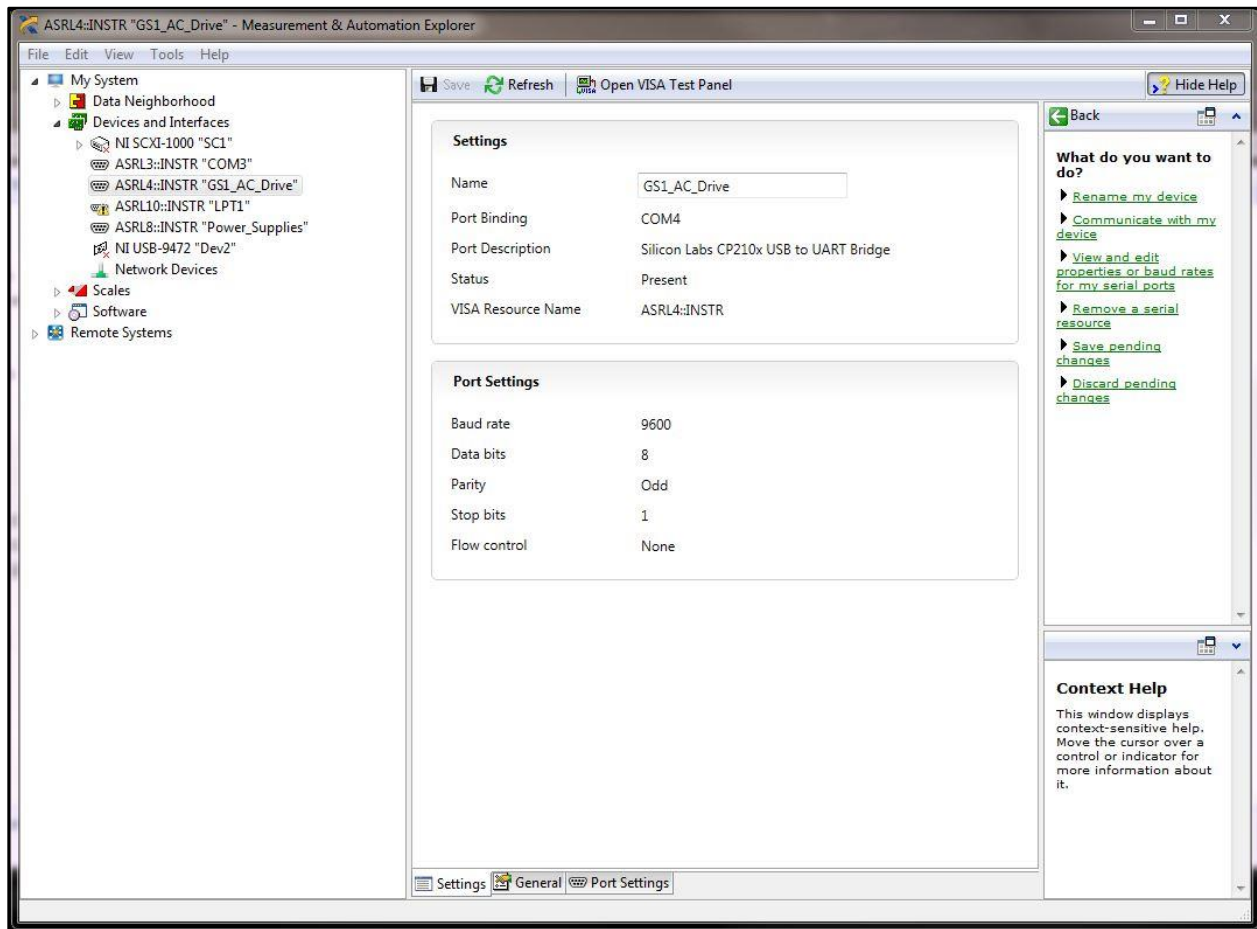


Figure 10. NI Measurement and Automation Explorer window, used to configure communication ports.

Remote communication with the VFD is done through Modbus, a serial communications protocol used commonly for connecting with industrial systems like programmable logic controllers. LabVIEW comes with a library of virtual instruments (VI) that allow for manipulation and use of Modbus protocol. Modbus can take one of two formats: ASCII or RTU. For CIET's VFDs, Modbus RTU was used.

In LabVIEW, the only Sub-VI that is necessary is the “MB Serial Mastery Query”, set to “Write Single Register” mode. A screenshot of an example block diagram of this Sub-VI can be seen in Figure 11. The critical inputs to this Sub-VI are the serial parameters (communication mode and address), the serial port name (also known as the VISA resource target), the address, and the holding register. The address and holding register are specific to the parameter that the user wants to manipulate; the address specifies the parameter, and the holding register is the value that is to be written to this parameter.

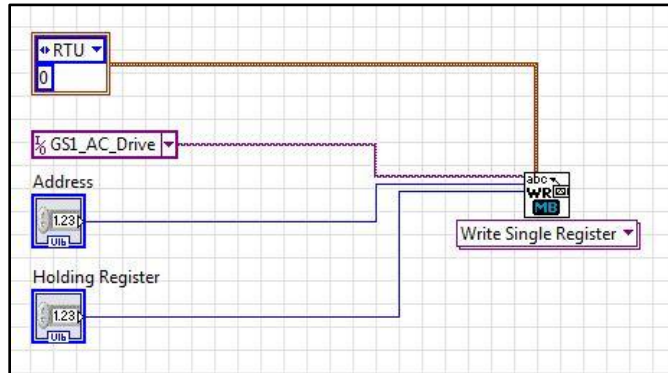


Figure 11. LabVIEW block diagram of the Modbus Sub-VI used to communicate with the VFDs.

The address of the parameter is related to the specified “Modbus Decimal” of each parameter, which is found in the GS1 user manual. For LabVIEW, the correct address for a parameter is as follows:

$$Address = Modbus\ Decimal - 40001$$

For example, P0.03 (Motor Base RPM) has a Modbus Decimal of 4004, which means that in LabVIEW the address should be 3. The holding register—the value that is to be written to the parameter—depends on the range and desired input. The range of values for each parameter can be found in the user manual.

There are certain critical parameters that are dependent on the type of motor that each VFD is controlling, and specific characteristics such as the necessary input current and the nameplate voltage. On CIET, there are some small differences between the motors on the fans and the motor on the pump. These parameters can be set from the computer. Table 2-5 shows the addresses and values that have to be sent through LabVIEW/Modbus to the VFD before the motors can be properly and safely controlled.

Table 2-5. Table of motor-dependent parameters that must be set before the VFD can properly control the motors.

Parameter	Description	Address	Holding Register	
			Pump	Fan
P0.00	Motor Nameplate Voltage	0	230	230
P0.01	Motor Nameplate Amps	1	16	13

CIET 1.0 I&C REPORT

P0.02	Motor Base Frequency	2	60	60
P0.03	Motor Base RPM	3	1725	1725
P0.04	Motor Maximum RPM	4	1725	1725
P6.15	Upper Bound of Output Frequency	1551	600	600
P6.16	Lower Bound of Output Frequency	1552	30	30

3 Feedback Control Theory

Feedback control systems use closed data loops to continuously manipulate a process according to measured error in a particular variable. The error is the difference between the actual measured value and the desired set-point of the value. The error is processed through a mathematical function and then determines how much a controlled variable should change in order to change the process to reduce the error. The fact that the measured variable is essentially sent “backward” upstream of the process is why this type of control system is called a “feedback” control system.

One simple example of a feedback control system would be a person driving a car. The driver gets information from the speedometer, and adjusts the car’s speed according to whether the speed is higher or lower than the desired speed by adjusting the pressure on the accelerator and the brake. The information on the car’s speed is continually fed back to the accelerator and brake positions via the driver.

The most popular way to implement a feedback controller is through a proportional-integral-derivative (PID) controller. A PID controller manipulates the controlled variable based on the error, the integral of the error, and the derivative of the error; each term is multiplied with a specific gain coefficient, and summed to get the final change to the controlled variable. The standard PID algorithm looks like this:

$$K_P e + K_I \int e dt + K_D \frac{de}{dt} = u(t)$$

Where K_P , K_I , and K_D are the proportional, integral, and derivative coefficients, respectively, and $u(t)$ is the change to the controlled variable.

The gain coefficients each affect the controller response in different ways, in accordance with the physical meaning of the error term they are multiplied with. The proportional term acts on the absolute distance between the actual and desired value of the process output, the integral term acts on the accumulation of error over time, and the derivative term acts on the speed of the process value change. For practical systems, another important variable is the actuation frequency, which is how often the algorithm executes and changes the controlled variable.

For many applications, a PID controller where some of the gain coefficients are zero is enough for rapid and consistent stability. A proportional (P) controller is one where only the proportional gain is non-zero; a proportional-integral (PI) controller is one where only the derivative gain is zero; and a proportional-derivative (PD) controller is one where only the integral gain is zero.

Most of the work around feedback control algorithm development involves tuning the gain and timing parameters for optimal system performance. There is a long history in developing theoretical tuning strategies for PID controllers that stretches back to the postwar era; strategies since then have become increasingly complex and nuanced, with different strategies applying to different types of systems and different needs for optimization. Some tuning strategies involve working with a mathematical model of the system; some involve tuning the controller while the

system is running; and some require running special tests to collect particular data sets around process dynamics. The following tuning strategies are discussed in this section:

- Trial-and-Error
- Ziegler-Nichols
- Relay feedback
- Process reaction curve
- Internal model control
- Integral of the time-weighted absolute value of the error for a first-order plus time delay model

3.1 Trial-and-Error Tuning

Trial-and-error tuning refers to manual tuning, where the user manually manipulates the gain coefficients of the control algorithm and observes subsequent performance. Different values for the PID coefficients and actuation frequencies are deployed, the process response is observed, and the values are changed according to the observed process response dynamics.

Some general guidelines are summarized in these rules, adapted from Sung et al. 2009:⁵

1. Large process output oscillations around the set-point mean that K_P is too large.
2. Long convergence times between the process output and the set-point mean that K_P is too small.
3. If, for a positive step-change, the process output oscillates above/below the set-point more than below/above the set-point, K_I is too large/small.
4. High-frequency oscillations of the process output mean that K_D is too small.

One key aspect of trial-and-error tuning is the need to have an estimate of the order of magnitude for the total gain of the controller for a given error; otherwise, an initial guess that is far from the ideal range of values could result in excessively unstable responses and possible damage to the system. Thus, it is very important to have a very good understanding of the general physics and dynamics of the system, either based on experience with manually actuating the controller or intuition on the theoretical dynamics underpinning the system's processes and characteristics.

3.2 Ziegler-Nichols Tuning

The Ziegler-Nichols (ZN) tuning rules were developed in 1942 by J.G. Ziegler and N.B. Nichols as a set of simple equations to find optimal control coefficients, based on the parameters

⁵ Su Whan Sung, Jietae Lee and In-Beum Lee, "Process Identification and PID Control", IEEE Press, John Wiley and Sons (Asia) Pte Ltd, 2009, pp151-54.

K_U and T_U , which are the ultimate gain and ultimate period of the process.⁶ These parameters are found by steadily increasing the gain of a P-Controller until the process is at the edge of stability, and recording the gain and the period of oscillation. There are also modified ZN tuning rules that have been developed in order to yield small overshoots and no overshoot.⁷ Table 3-1 lists out the various ZN tuning rules.

Table 3-1. List of Ziegler-Nichols tuning rules, based on the ultimate gain and ultimate period

<i>Controller Type</i>	K_p	K_I	K_D
P	$0.5K_U$	–	–
PI	$0.45K_U$	$1.2K_p/T_U$	–
PD	$0.8K_U$	–	$K_p T_U/8$
PID	$0.6K_U$	$2K_p/T_U$	$K_p T_U/8$
PID (Some Overshoot)	$0.33K_U$	$2K_p/T_U$	$K_p T_U/3$
PID (No Overshoot)	$0.2K_U$	$2K_p/T_U$	$K_p T_U/3$

3.3 Relay Feedback

Relay feedback tuning was developed in 1984 by K.J. Astrom and T. Hagglund as a way to avoid the problem of operating near unstable regions in order to find the ultimate gain of the process.⁸ Relay feedback involves creating a square wave function that actuates the controller, thus creating an oscillation in the process output, which in turn feeds back to the square wave to determine its period. The resulting oscillations’ amplitude and period are used to calculate the ultimate gain and ultimate period, which are then used to calculate the PID coefficients. A graph of the inputs and outputs of the relay can be seen in Figure 12.

⁶ J.G. Ziegler and N.B. Nichols, “Optimum Settings for Automatic Controllers”, *Transactions of the American Society of Mechanical Engineers*, 64, pp759-768, 1942.

⁷ Anthony S. McCormack and Keith R. Godfrey, “Rule-Based Autotuning Based on Frequency Domain Identification”, *IEEE Transactions on Control Systems Technology*, Vol 6, No 1, 1998.

⁸ K.J. Astrom and T. Hagglund, “Automatic Tuning of Simple Regulators with Specifications on Phase and Amplitude Margins”, *Automatica*, 20, 5, pp645-651, 1984.

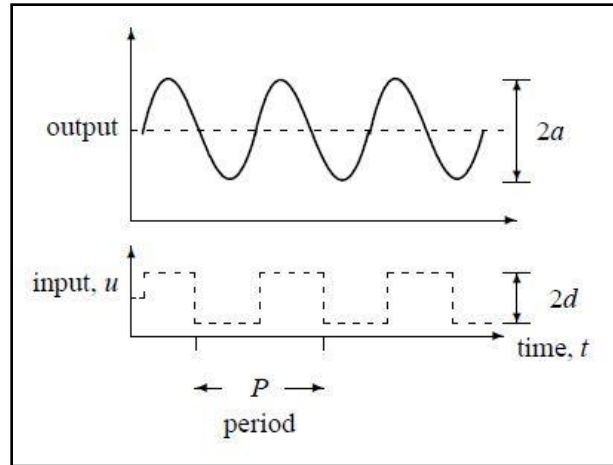


Figure 12. Graph of controller input and process output during relay feedback operation.⁹

Given that d is the amplitude of the input relay (which is user determined), a is the amplitude of the process output, and P is the observed period of the oscillation, the ultimate gain and period are as follows:

$$K_U = \frac{4d}{\pi a}$$

$$T_U = P$$

These values are then applied to the same algorithms used for standard ZN tuning.

3.4 Process Reaction Curves for Model Construction

The process reaction curve (PRC) method is a simple process identification strategy to develop a first-order plus time delay (FOTD) model of the process, which can then be used to derive optimal PID coefficients. The method finds the coefficients to the following equation, which is in the frequency domain:

$$G(s) = \frac{ke^{-\theta s}}{\tau s + 1}$$

Where k is the static gain, θ is the time delay, and τ is the time constant of the response.

The PRC method analyzes the response of the process to a step-change in the controller. The static gain is calculated as the ratio of the change in the controller value to the change in the process. The time delay is the difference between the time at which the controller value is changed and the time when the process response begins. The time constant is the difference

⁹ D.I. Wilson, "Relay-based PID Tuning", *Automation and Control*, 2005.

between the time when the process response begins, and the time when the process response has reached 63.2% of the final change in process value.

The FOTD coefficients can be used to derive optimal PID coefficients using model-based tuning rules.

3.5 Internal Model Tuning

The Internal Model Control (IMC) tuning rule, also known as the lambda tuning rules, are effective at set-point tracking, but sluggish at rejecting disturbances. The IMC tuning rules for a PID controller as are follows:

$$K_P = \frac{1}{k} \frac{2\tau + \theta}{2(\lambda + \theta)}$$

$$K_I = \frac{K_P}{\tau + \frac{\theta}{2}} = \frac{1}{k} \frac{2\tau + \theta}{2(\lambda + \theta)(\tau + \frac{\theta}{2})}$$

$$K_D = K_P \frac{\tau\theta}{2\tau + \theta} = \frac{1}{k} \frac{2\tau + \theta}{2(\lambda + \theta)} \frac{\tau\theta}{2\tau + \theta}$$

Where $\lambda \geq 0.25\theta$.

3.6 ITAE-1

The integral of the time-weighted absolute value of the error for a FOTD model (ITAE-1) tuning rules have two different sets of equations for PID tuning, depending on whether the primary goal is set-point tracking or disturbance rejection. The ITAE-1 tuning rules for disturbance rejection are as follows:

$$K_P = \frac{1}{k} 1.357 \left(\frac{\theta}{\tau}\right)^{-0.947}$$

$$K_I = \frac{K_P}{\tau_I} = \frac{1}{k\tau} 1.357 \left(\frac{\theta}{\tau}\right)^{-0.947} 0.842 \left(\frac{\theta}{\tau}\right)^{-0.738}$$

$$K_D = K_P \tau_D = \frac{\tau}{k} 1.357 \left(\frac{\theta}{\tau}\right)^{-0.947} 0.381 \left(\frac{\theta}{\tau}\right)^{0.995}$$

4 Application and Results for CIET Controllers

This section reviews the application of various feedback control development theories and practices, discussed in Section 3, to the four controllers in CIET, as well as the results and recommendations. The four controllers are the power supplies, pump, CTAH, and TCHX. The power supplies used their own, unique feedback control algorithm based on Ohm's Law and resistance measurements. The pump was found to be best controlled by a P controller. A variety of different tuning strategies were tested for CTAH, in order to both find the optimal control algorithm for CTAH and gain experience with the strategies best suited to tune an air-cooled heat exchanger. It was found that relay feedback control was the most effective and efficient tuning strategy for CTAH, and this was subsequently applied to TCHX.

4.1 Power Supplies

The control strategy for the power supply is distinct from the strategies used for other controllers in that there is no PID controller; rather, it is in the form of an open-loop controller that continually changes the value of the voltage limit based on the measured resistance value. This is the optimal strategy because there is a known and accurate mathematical relationship between resistance, voltage, current, and power, that can be used to determine the exact voltage needed to achieve a target power input. Continual monitoring of the resistance is necessary because the resistance increases as the heater temperature rises; thus, open-loop control based on a constant value of the resistance results in errors at higher powers and temperatures.

The resistance-based feedback control algorithm is based on Ohm's Law:

$$V = IR; P = IV = \frac{V^2}{R}$$

where V is the voltage, I the current, R the resistance, and P the power.

The equation for determining the voltage limit in a given iteration is as follows:

$$V_L = \frac{1}{2} \sqrt{P_{sp} R_{i-1}} = \frac{1}{2} \sqrt{P_{sp} \left(\frac{V_1}{I_1} + \frac{V_2}{I_2} \right)_{i-1}}$$

where the L subscript stands for the applied limit, the sp subscript the set-point, the $i - 1$ subscript the previous iteration, and the numeric subscript the power supply (1 or 2). All values that are not applied limits refer to the measured value; all values that are not of the previous iteration are values of the present iteration.

The resistance feedback algorithm reduced the errors associated with the open-loop control. Figure 13 shows graphs of the power set-point, actual power output, and percent errors associated with each control strategy. The spikes in the error graphs are associated with set-point changes. Steady-state error for the open-loop algorithm was in the range of approximately 2%, whereas the error associated with the resistance feedback algorithm was well under 1%.

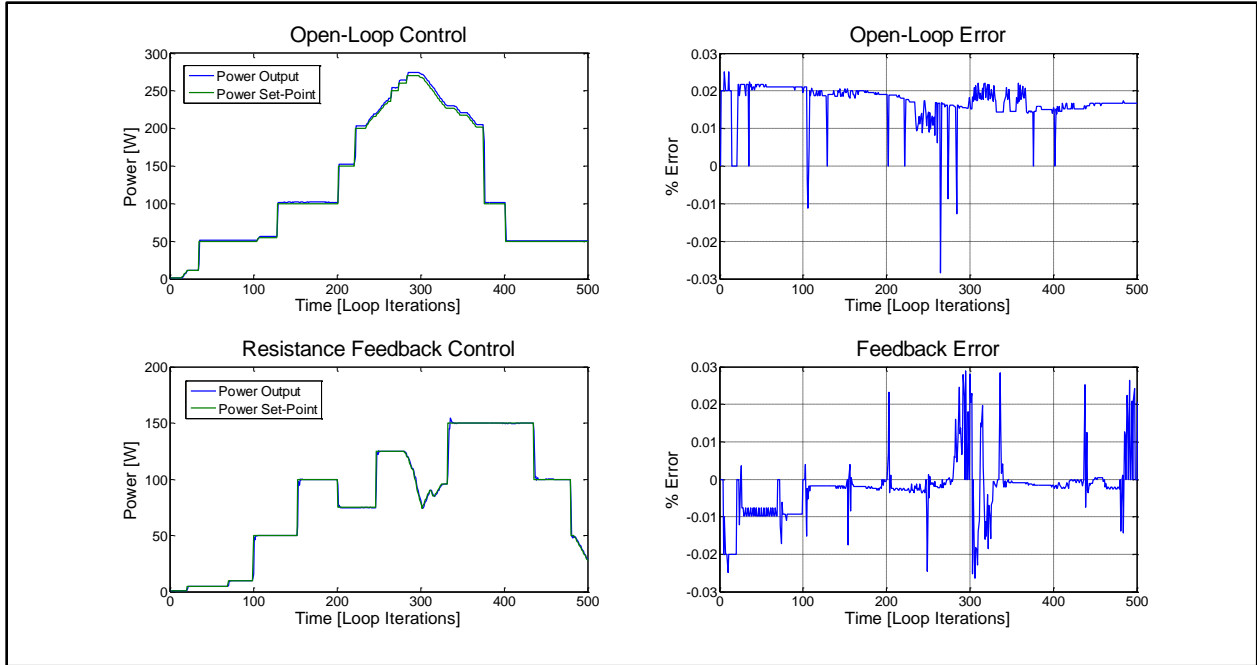


Figure 13. Graphical comparison of open-loop and resistance feedback control strategies for the power supplies.

4.2 Pump

The pump uses a proportional controller to achieve the desired mass flow rate in the primary loop. The algorithm is as follows:

$$f_i = f_{i-1} + K_p(m_{sp} - m)$$

Where f stands for the pump VFD's frequency, K_p is the proportional coefficient, and m is the mass flow rate; the i subscript stands for the iteration, and the sp subscript stands for the set-point.

An estimated optimal value for K_p can be calculated from theoretical predictions of pump performance for various rotational speeds and temperatures, as given in technical and support documents for the pump. Figure 14 shows the graph of the pump curve, which can be used to estimate the relationship between the rotational speed and the volumetric flow rate.

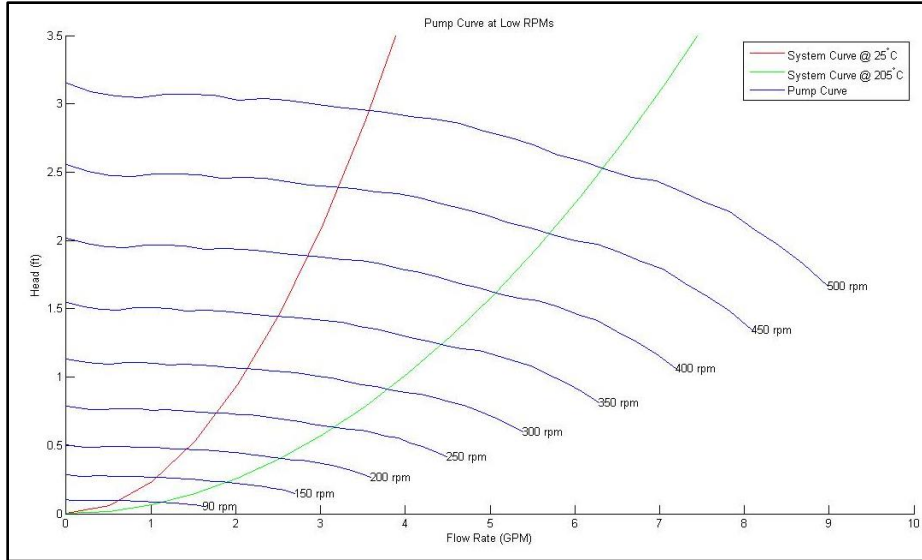


Figure 14. Pump curve from technical sheet.

From qualitative analysis of the pump curves, the relationship between changing the RPM and a change in gallons per minute (GPM) is found to be in the following range, assuming temperatures between 25°C and 115°C:

$$\pm 50 \text{ RPM} = \pm 0.33 \text{ to } 0.39 \text{ GPM}$$

The conversion factor between *GPM* and *kg/s* is as follows:

$$\frac{\text{gallon}}{\text{minute}} = (264.172 \frac{\text{gallons}}{\text{m}^3}) (60 \frac{\text{s}}{\text{minute}}) (\frac{1}{1056} \frac{\text{kg}}{\text{m}^3})$$

Where $1056 \frac{\text{kg}}{\text{m}^3}$ is the density of Dowtherm A at 25°C.

The conversion factor between frequency and RPM is as follows:

$$60 \text{ Hz} = 1725 \text{ RPM}$$

Thus, using all of these conversion factors, an optimal stable range for K_p can be found:

$$K_p \left[\frac{\text{Hz}}{\text{kg/s}} \right] = \left(\frac{60 \text{ Hz}}{1725 \text{ RPM}} \right) \left(\frac{50 \text{ RPM}}{0.33 - 0.39 \text{ GPM}} \right) \left(\frac{15 \text{ GPM}}{\text{kg/s}} \right) = 67 - 79 \frac{\text{Hz}}{\text{kg/s}}$$

Large gains create overshoot and possible instability; small gains create sluggish controls and long convergence times between the set-point and the process output. It is also important to note the importance of the controller timer when developing a feedback control algorithm. The frequency of the controller actuation has a large effect on the controller dynamics, due to lag times between a change in the controller output and a change in the process output.

A range of gain values around the theoretical stable range was tested, for both set-point step-up and step-down scenarios. Figure 15 shows the controller performance for gains between 500

and 1200, for a step-up of the mass flow-rate set-point from 0.1 kg/s to 0.18 kg/s. It was found that the gain values of 790 and 900 exhibited the best performance, given that they rapidly converged with the set-point of 0.18 kg/s with little to no overshoot. Figure 16 shows the controller performance for gains between 500 and 900, for a step-down of the mass flow-rate set-point from 0.18 kg/s to 0.1 kg/s. It was found that only the lowest tested gain, 500, did not result in an undershoot, and all gains above 600 resulted in an undershoot of over -0.01 kg/s. These results demonstrate that a gain that is optimal for a step-up in the set-point is not necessarily optimal for a step-down in the set-point, and thus it is necessary to find a gain that give acceptable performance for both types of set-point changes.

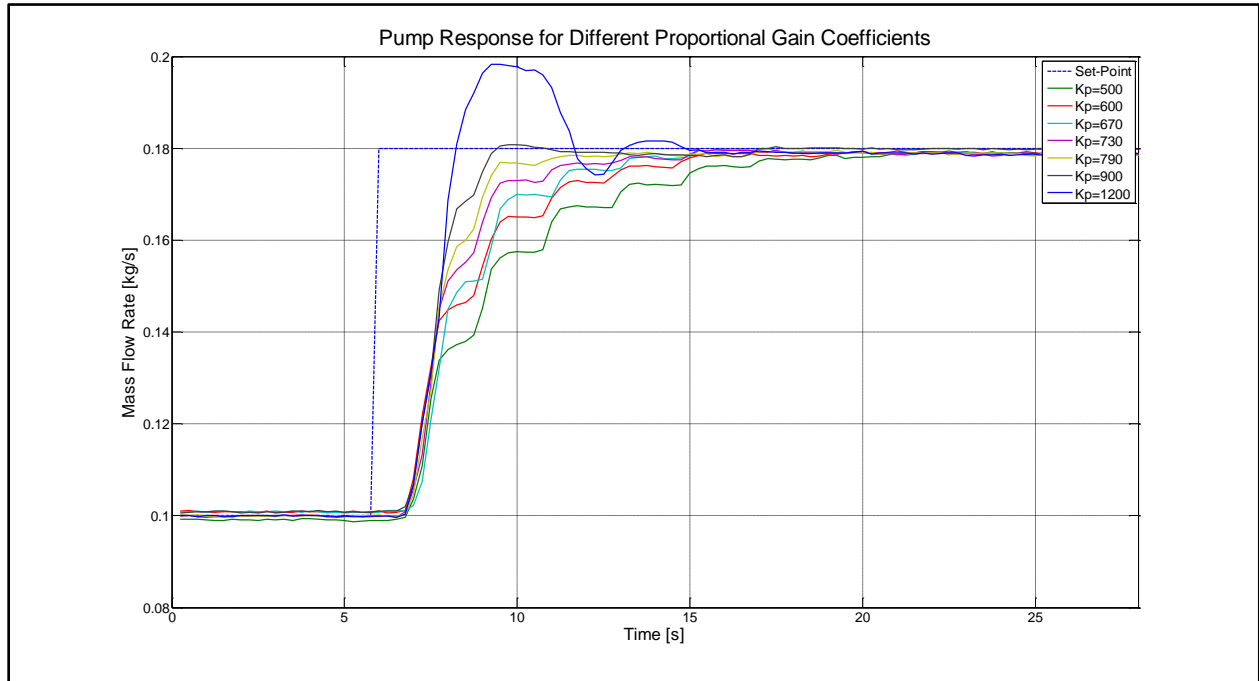


Figure 15. Pump response for a set-point change from 0.1 kg/s to 0.18 kg/s, for a range of proportional gain coefficients for an actuation frequency of 2 s.

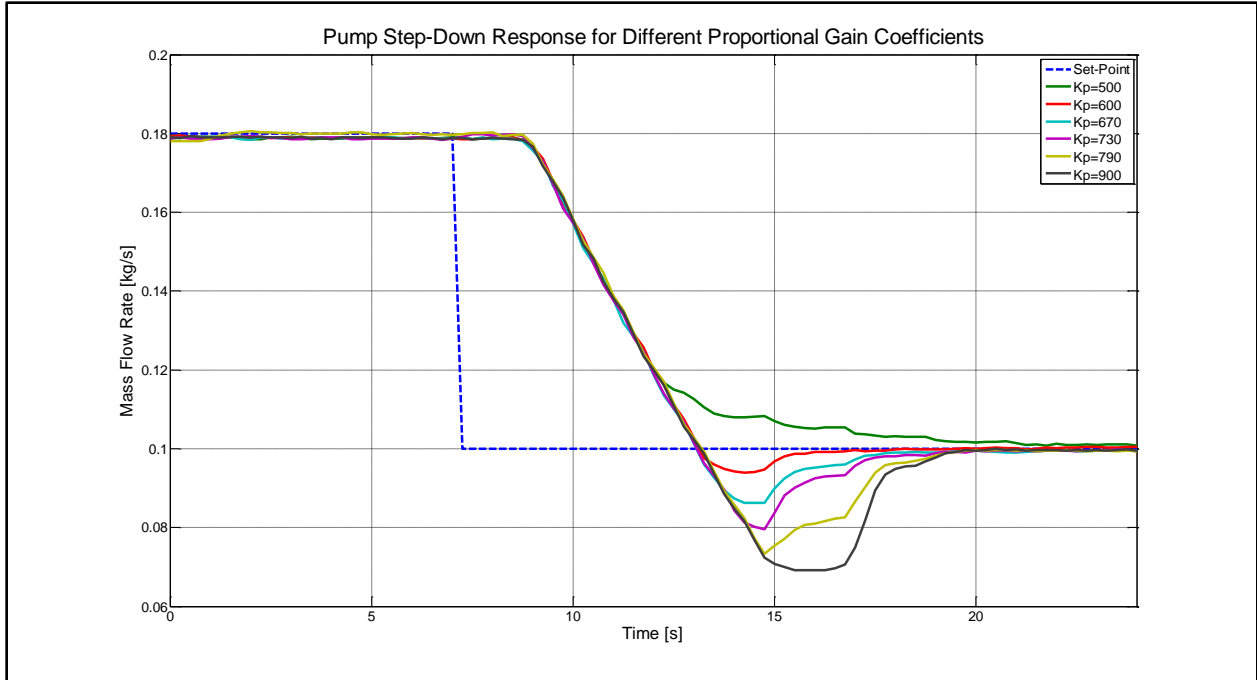


Figure 16. Pump response for a set-point change from 0.18 kg/s to 0.1 kg/s, for a range of proportional gain coefficients for an actuation frequency of 2 s.

It is also important to recognize the effect of the actuation frequency on controller performance. Higher actuation frequencies will generally result in more instability and oscillation for the same set of gain coefficients; this is because the faster the controller is sampling the error, the less time the controller is giving for the response of the last actuation to actually affect the error. Thus, higher actuation frequencies (lower actuation timers) will consistently over-estimate the error and create overshoot. Figure 17 shows the controller performance for three different actuation frequencies, for a proportional gain of 730. While actuation timers of two seconds and three seconds yield similar responses, a timer of 1 second yields a significant overshoot.

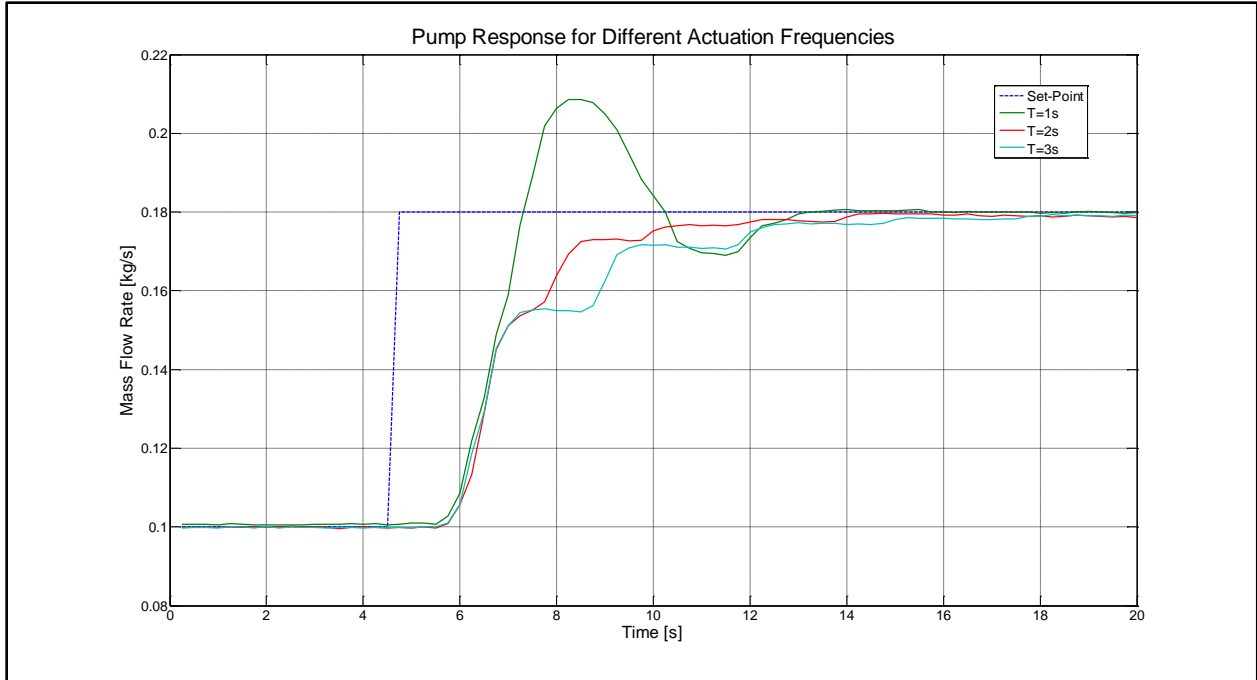


Figure 17. Pump response for a set-point change from 0.1 kg/s to 0.18 kg/s, for a range of actuation frequencies for a proportional gain of 730.

4.3 CTAH

The primary goal of the CTAH is to control the outlet temperature of the heat exchanger. The CTAH was tested with various PID controllers, and in a variety of different operational states. The main variables influencing the CTAH outlet temperature are the power input, the average temperature across the heater, and the mass flow rate. Manual tuning results were tested with a variety of conditions and types of disturbances. More complex tuning results were tested primarily with controlling the start-up process for rapid and stable convergence with normal steady-state conditions.

4.3.1 Manual Tuning

Initial estimates for stable gain values for the feedback controller were done by changing the frequency manually and observing the outlet temperature response. These initial tests were done with a power input of 1 kW, a mass flow rate of 0.18 kg/s, average temperatures in the range of 40°C, and a ΔT in the range of 5°C. It was observed that a frequency change of 7.5 Hz resulted in an outlet temperature change of 3°C; thus, given the aforementioned conditions, the proportional gain should be on the order of $\frac{2.5 \text{ Hz}}{^\circ\text{C}}$, or 25. In general, this initial observation was used for the baseline prediction that the range of optimal gain for any CIET state would be in the range of 1 – 50.

A proportional controller with a proportional gain of 10 and an actuation frequency of 20 s was tested for a situation where the mass flow rate is 0.18 kg/s and the outlet set-point is 50°C.

This controller was able to stabilize the outlet temperature after the initial heat-up, and was able to stabilize the outlet temperature in response to a step-increase of 1 kW in heater power, from 3 kW to 4 kW. The results can be seen in Figure 18.

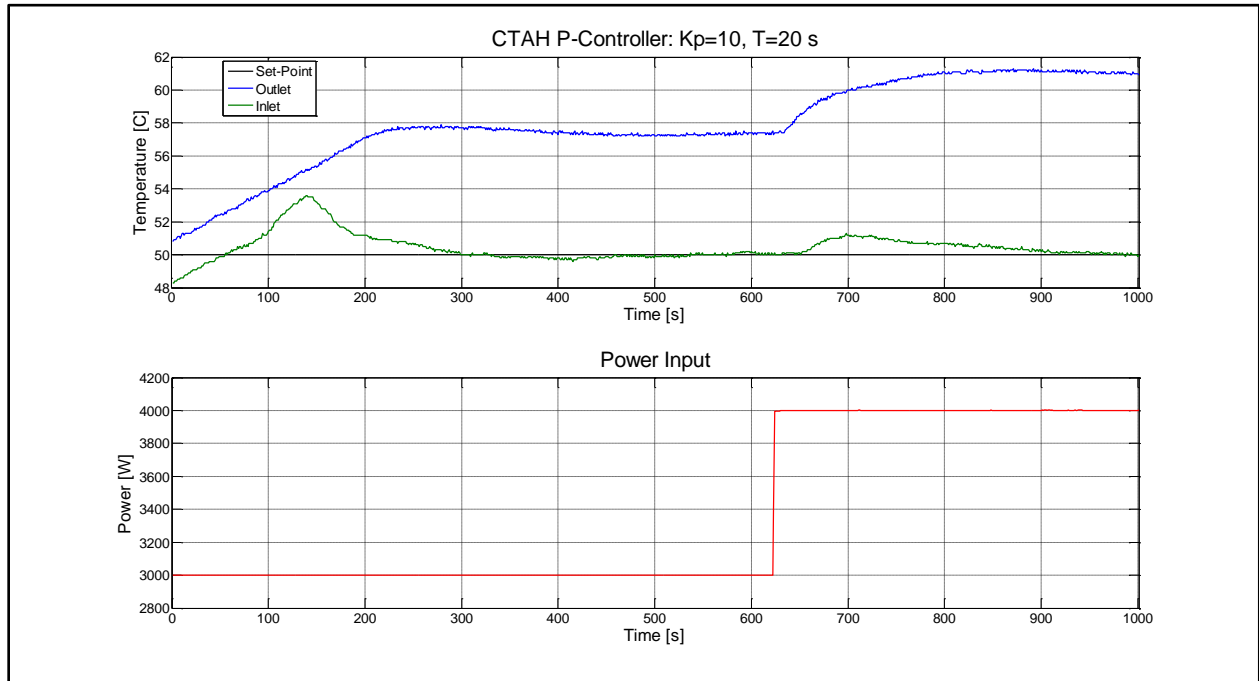


Figure 18. CTAH outlet temperature response for a proportional controller with a gain of 10 and an actuation frequency of 20 s, during a heat-up and power step-change scenario.

This same controller was tested at higher temperatures and with a power input of 6 kW, for a set-point of 75°C, and performed well. The actuation frequency was then decreased to 10 s, and the set-point was stepped-down to 70°C, and this slightly modified controller was also stable. The results can be seen in Figure 19.

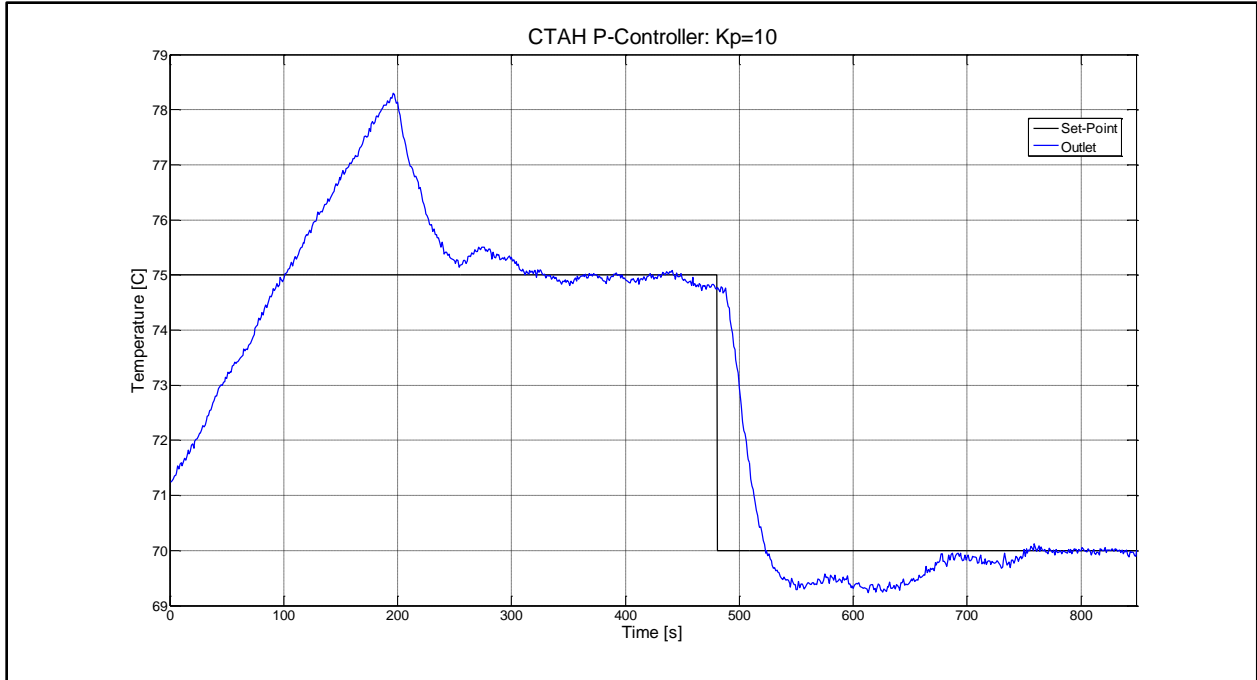


Figure 19. CTAH outlet temperature response of two controllers. The actuation frequency was 20 s for the set-point of 75°C, and 10 s for the set-point of 70°C.

While this controller ($K_p = 10, T = 10 \text{ s}$) works well at higher flow rates, its performance is severely degraded at lower flow rates. One test was performed with the power at 2 kW and the outlet temperature set-point at 46°C, and a disturbance in the form of a step-down in the mass flow rate from 0.18 kg/s to 0.10 kg/s, as seen in Figure 20. At the lower mass flow rate, the outlet temperature exhibited far more oscillation than at the higher mass flow rate, and took roughly three times as long to converge. Physically, this degraded controller performance is tied to the fact that lower mass flow rates result in longer time lags between the controller and the process; thus, increasing the controller actuation timer should improve performance. Figure 21 shows the controller response to a further step-down in the mass flow rate, with a timer of 30 s, and performance was significantly improved, with fewer oscillations and a shorter convergence time.

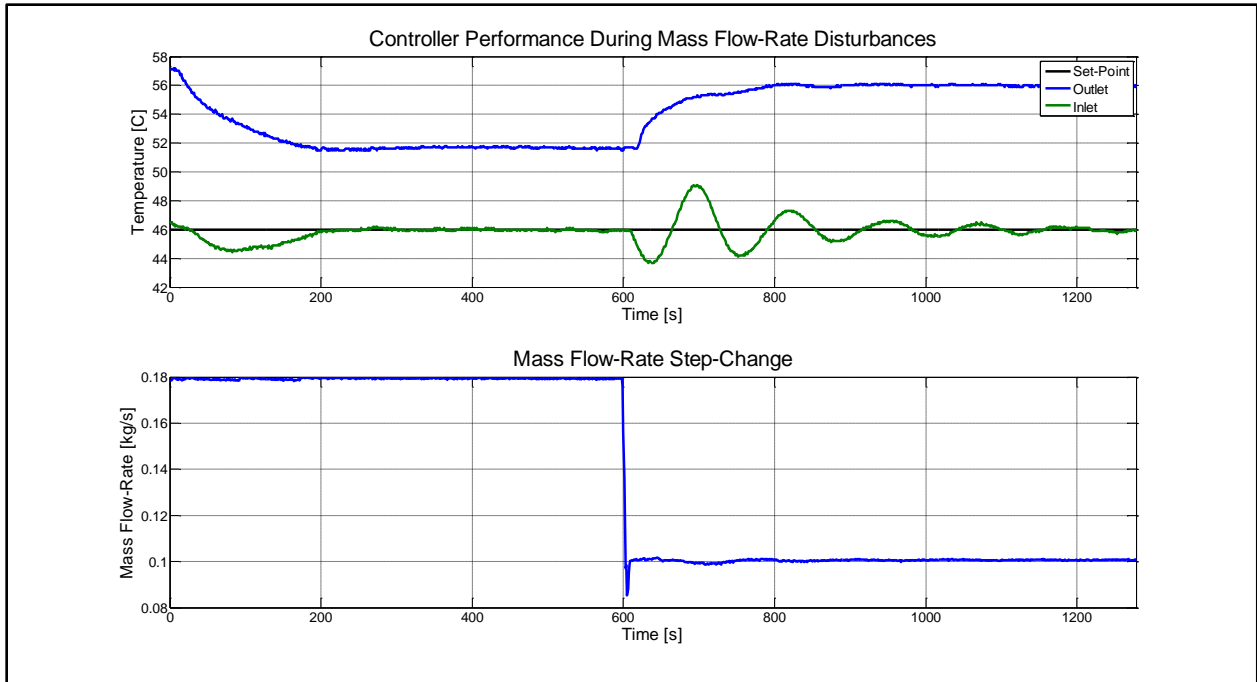


Figure 20. CTAH outlet temperature response to a step-change in the mass flow-rate, for a P-Controller with a proportional gain of 10 and an actuation timer of 10 s.

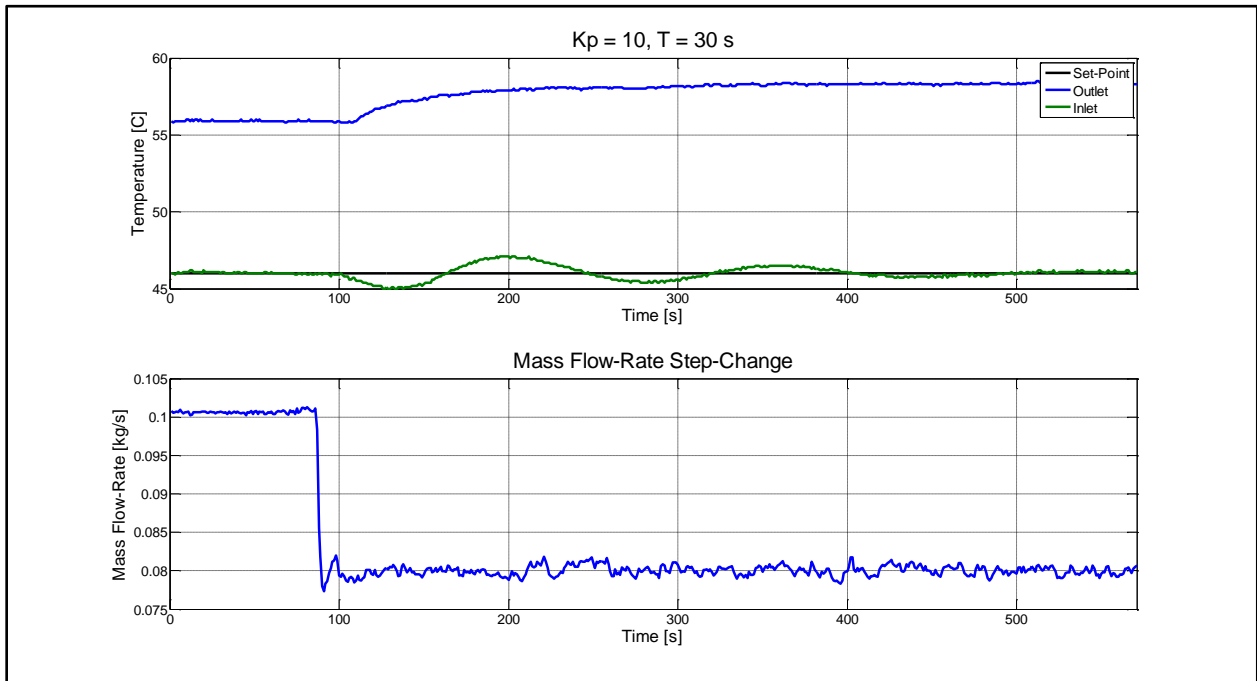


Figure 21. CTAH outlet temperature response to a step-change in the mass flow-rate from 0.10 kg/s to 0.08 kg/s, for a P-controller with a proportional gain of 10 and an actuation timer of 30 s.

A PD-Controller ($K_P = 3, K_D = 100 T = 30 s$) was tested at very low mass flow rates, at which natural circulation dominates and the pump is turned off. As characteristic of PD controllers, the outlet temperature was relatively stable but had noticeable error, as seen in Figure

22. Figure 23 compares the outlet temperature response of the P-Controller and the PD-Controller.

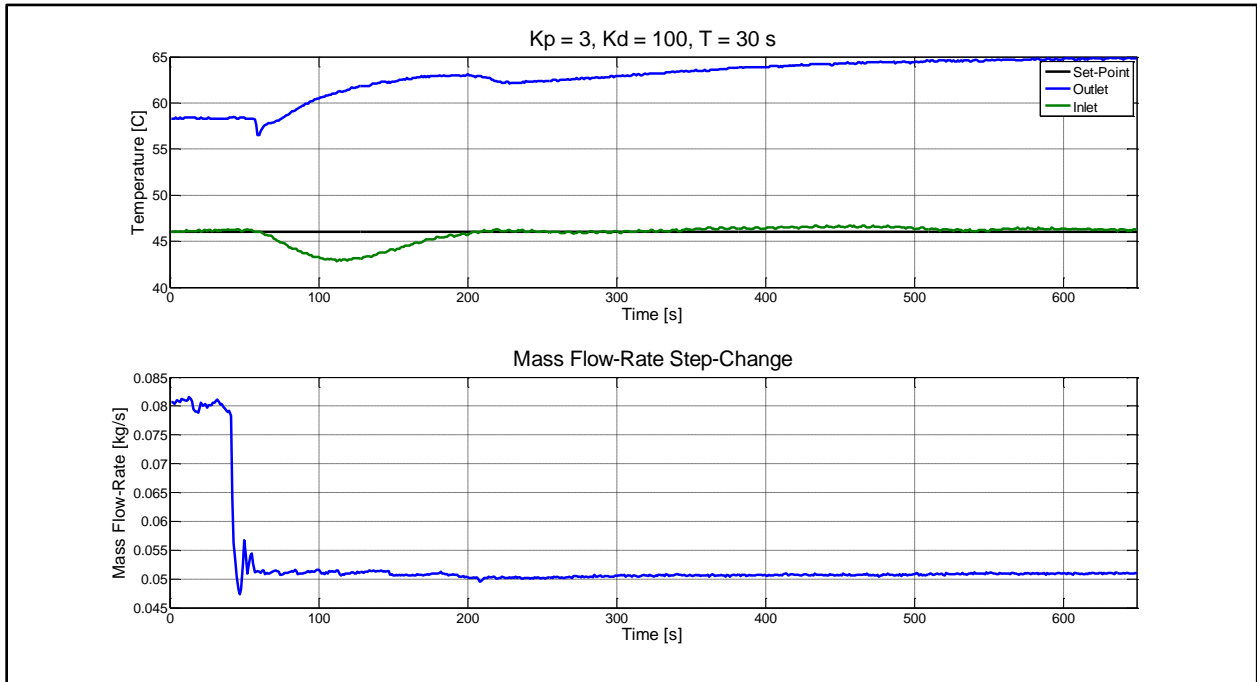


Figure 22. CTAH outlet temperature response to a step-change in the mass flow-rate from 0.08 kg/s to 0.05 kg/s, for a PD-Controller with a proportional gain of 3, a derivative gain of 100, and an actuation frequency of 30 s.

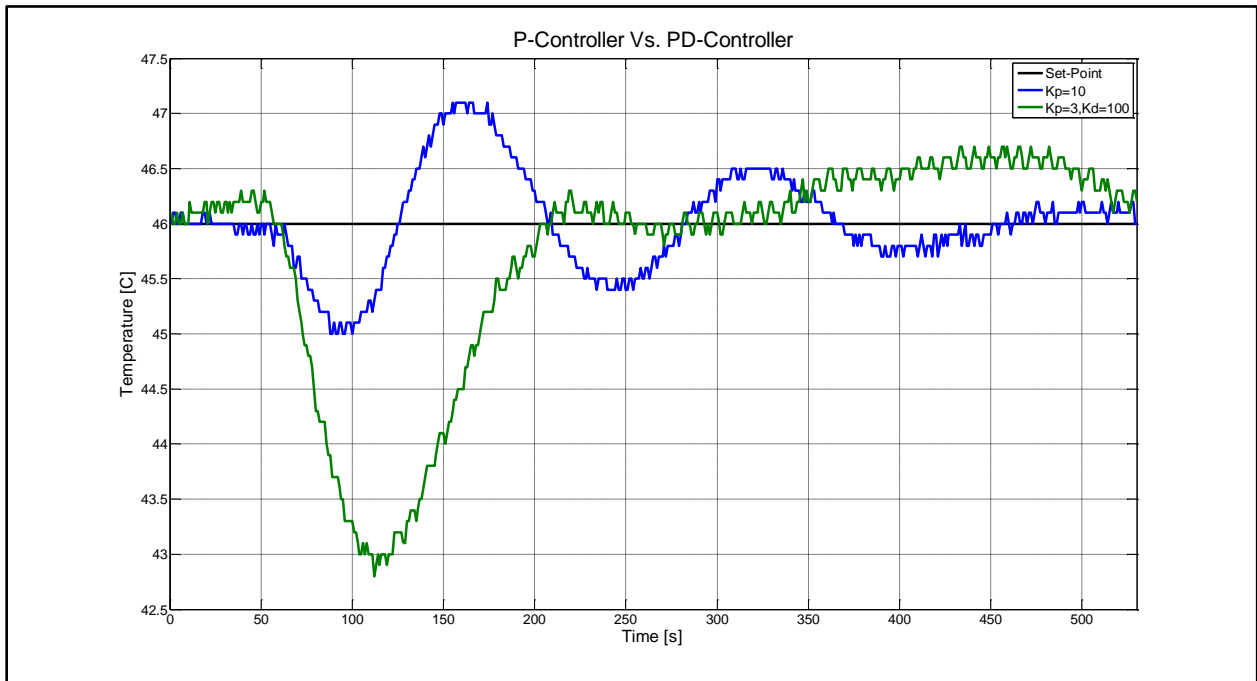


Figure 23. Comparison of the CTAH outlet temperature response when controlled by a P and a PD controller, each with an actuation frequency of 30 s.

Testing demonstrated that a proportional coefficient of 10, with an actuation timer dependent on the operational state, would be effective at controlling the CTAH outlet temperature. For normal operation of CIET, the most critical state for control is during start-up, when the system is heating up to normal, steady-state mode. Here, the power level is high (between 6 – 10kW), the mass flow rate is 0.18 kg/s, and the outlet temperature target is 80°C. It was found that a timer of 15 s would enable effective control, whereas a shorter timer would result in oscillations and possible instability. Figure 24 compares the outlet temperature response during start-up for an actuation frequency of 10 s and 15 s.

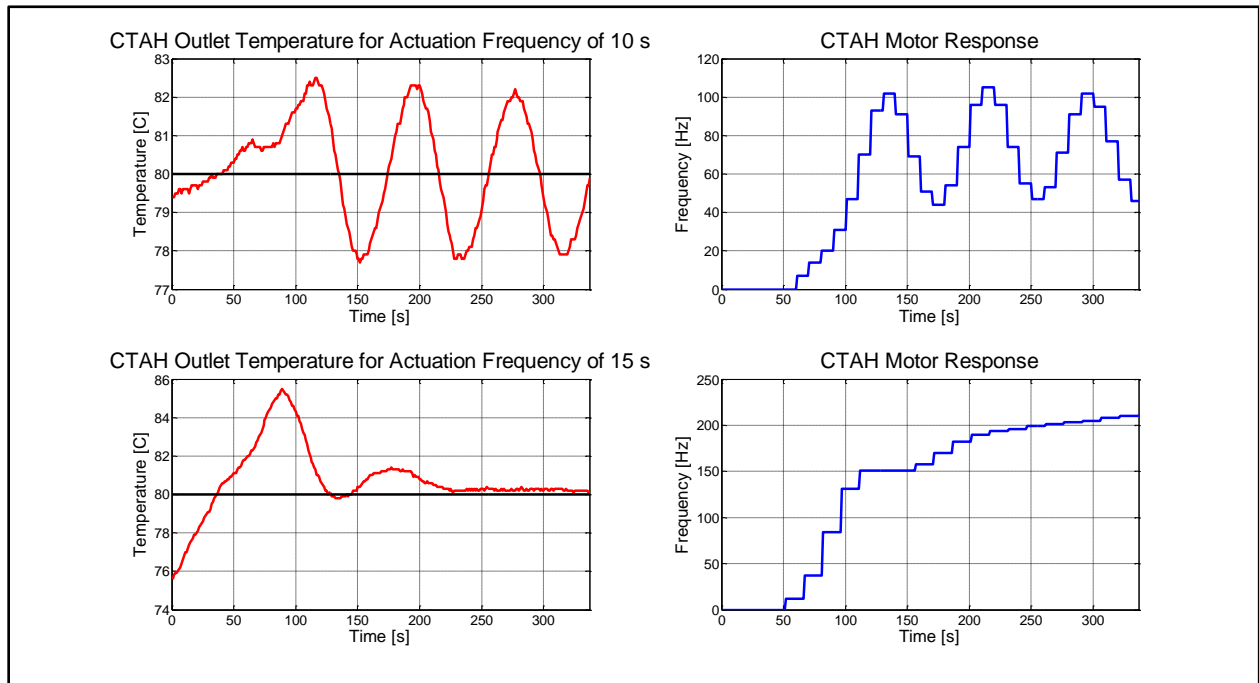


Figure 24. CTAH outlet temperature and motor responses for two different actuation frequencies, given a proportional gain of 10 and an outlet temperature set-point of 80 C.

A P-Controller with a proportional coefficient of 10 and a timer of 15 s was also effective at rejecting disturbances from power step changes with minimal to no overshoot. Figure 25 shows the performance of this controller for several different power-step changes, and Figure 26 shows the CTAH motor response for this test.

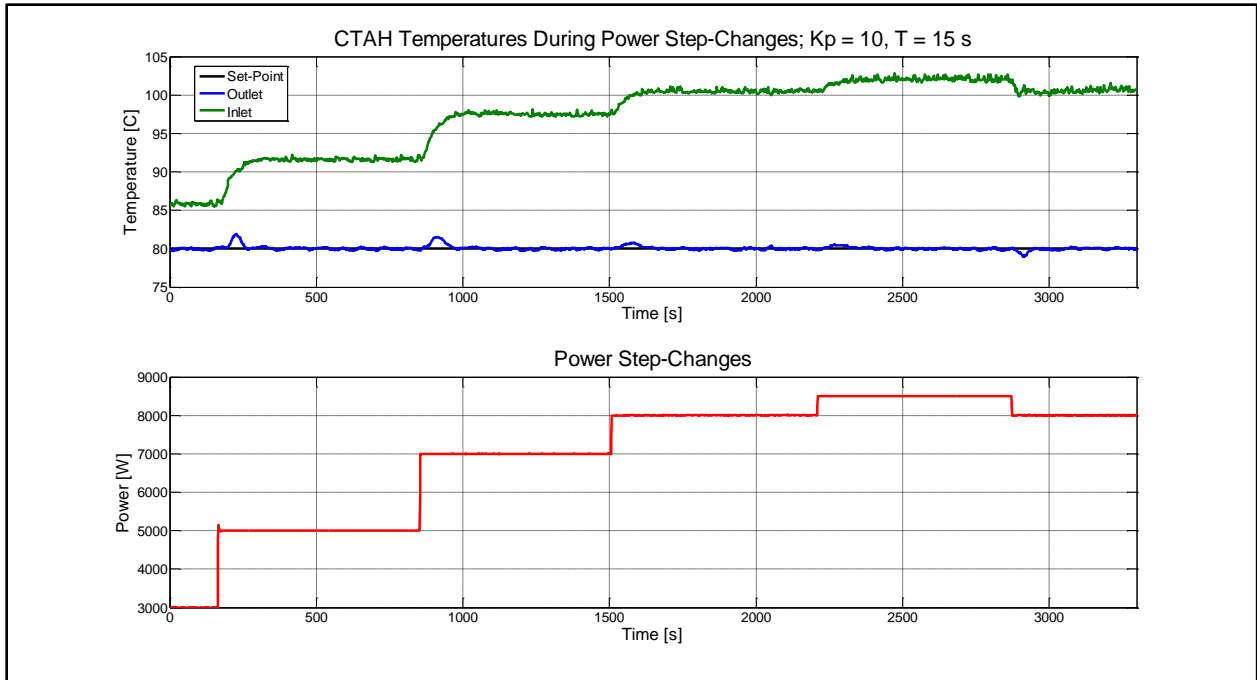


Figure 25. CTAH temperature response to power step-changes, with the outlet temperature controlled with a P-Controller with proportional gain of 10 and an actuation frequency of 15 s.

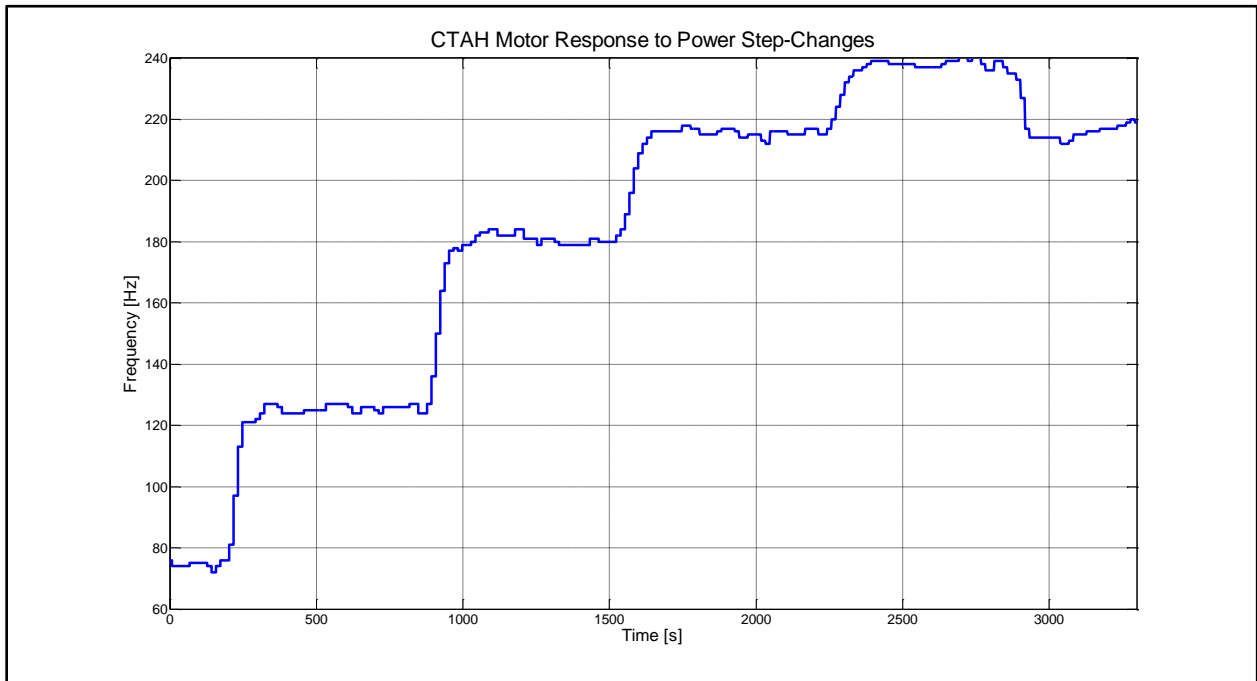


Figure 26. CTAH motor response to power step-changes, with aforementioned conditions.

4.3.2 Process Reaction Curve, Model Construction, and Model-Based Tuning

The PRC test was performed with the CTAH outlet temperature at 80°C, the mass flow rate at 0.18 kg/s, and the power input at 6 kW, and with frequency step-changes of 0.5 Hz and

5.0 Hz. Figure 27 shows the outlet temperature response to a +5.0 Hz step-change in the frequency, from 15.0 Hz to 20.0 Hz.

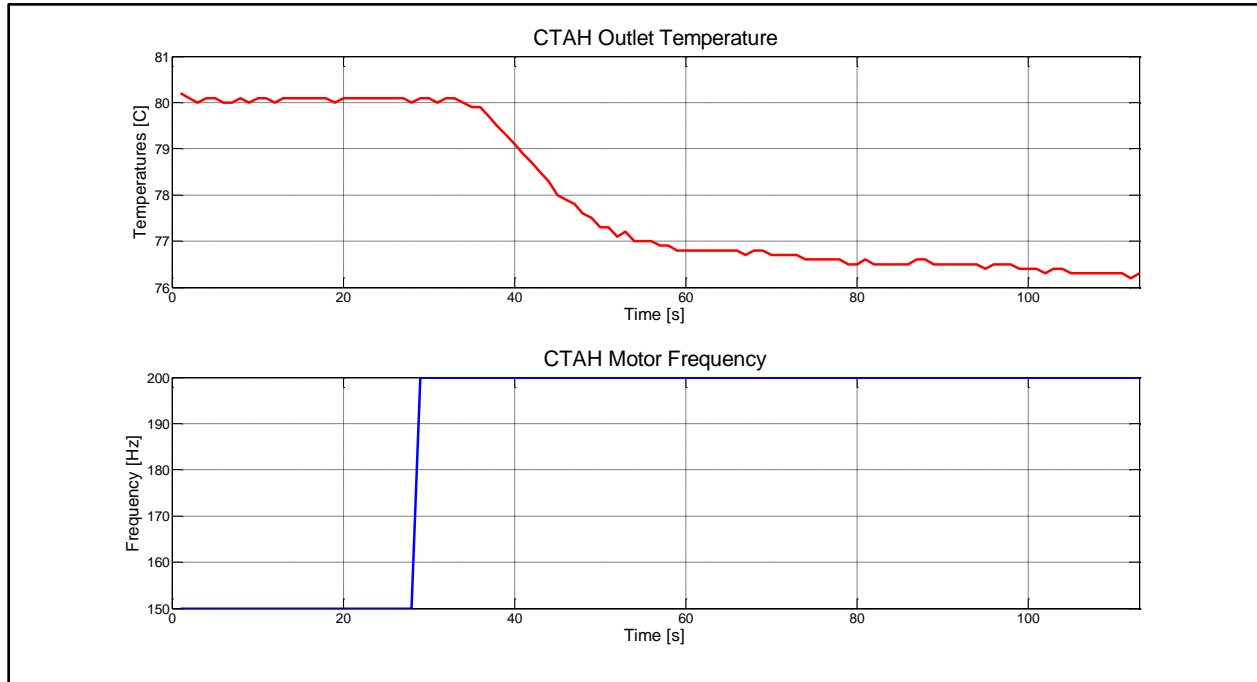


Figure 27. PRC test at normal, steady-state conditions with a frequency step-change of +5.0 Hz.

There are two parts to the CTAH outlet temperature response from a frequency step-change: the first part is the immediate change in the temperature difference between the inlet and outlet temperatures that results from the change in frequency, and the second part is a longer-term response that results from a general cooling of the system and a decreasing inlet temperature. For CTAH’s PRC analysis, only the first response is analyzed, since the feedback control strategy relies on the primary short-term response and not the secondary long-term response.

From the test, it is found that the initial and final temperature (approximate) of the CTAH outlet is 80.1°C and 76.5°C, or a temperature change of 3.6°C. Thus, the static gain term of the FOTD model can be found:

$$k = \frac{y_{\infty} - y}{d} = \frac{\Delta T}{\Delta f} = \frac{3.6^{\circ}\text{C}}{50 \text{ Hz}} = 0.072$$

The frequency step-change takes place at $t = 30 \text{ s}$, and the outlet temperature response begins at $t = 37 \text{ s}$. Thus, the time delay can be found:

$$\theta = 37 - 30 = 7 \text{ s}$$

The time constant is the time it takes for the outlet temperature to reach 63.2% of the temperature change, which corresponds to the time between the beginning of the outlet temperature response and the time at which the outlet temperature has dropped by 2.3°C, and is at 77.8°C. The outlet temperature is at this point at $t = 48 \text{ s}$. Thus, the time constant can be found:

$$\tau = 48 - 37 = 11 \text{ s}$$

This PRC analysis was done for several other step-changes, the results of which are seen in Table 4-1. The tests were all performed with CIET roughly at normal, steady-state conditions, with the average temperature across the CTAH around 87°C, the power input at 6 kW, and the mass flow rate at 0.18 kg/s.

Table 4-1. Results of PRC testing on CTAH at normal, steady-state conditions.

Motor Frequency Step-Change	k	θ	τ
+5.0 Hz	0.072	7	11
-5.0 Hz	0.09	8	13
-0.5 Hz	0.06	8	9

The FOTD coefficients were then plugged into the IMC and ITAE-1 tuning equations to derive theoretically optimal PID coefficients. Table 4-2 shows the derived PID coefficients for each of the PRC tests for the two sets of tuning rules.

Table 4-2. Theoretically optimal PID coefficients based on FOTD-based tuning rules.

Motor Frequency Step-Change	IMC			ITAE-1		
	K_P	K_I	K_D	K_P	K_I	K_D
+5.0 Hz	23	1.59	61	29	3.09	77
-5.0 Hz	19	1.11	58	24	2.21	73
-0.5 Hz	22	1.67	60	25	2.58	77

The two tuning rules yield similar PID controllers, with the ITAE-1 tuning rules yielding slightly larger coefficients. In order to account for the fact that the dynamics of the outlet temperature are different depending on whether the temperature is cooling or heating, the PID controllers that were tested were averaged between the results found from the 5.0 Hz step-change tests. Table 4-3 shows the PID coefficients that were tested.

Table 4-3. PID coefficients derived from FOTD model-based tuning rules that were selected for testing.

Controller Type	K_P	K_I	K_D
IMC	21	1.35	60
ITAE-1	26	2.65	75

These controllers were tested for their ability to control the CTAH outlet temperature during start-up, in conditions identical to those that were used during the PRC test: power input was 6 kW , the mass flow-rate was 0.18 kg/s , and the outlet temperature set-point was 80°C . Figure 28 shows the resulting graphs of the temperatures and the motor frequency.

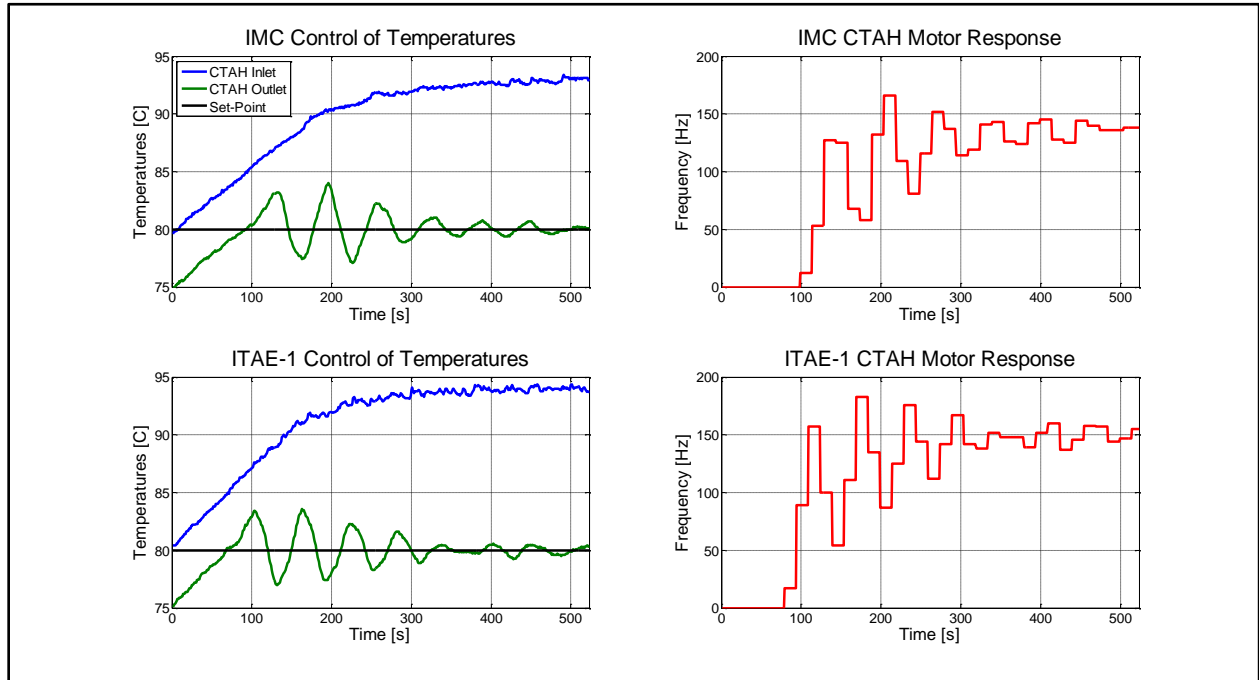


Figure 28. Comparison of IMC and ITAE-1 PID controllers during CIET start-up.

Neither the IMC nor the ITAE-1 tuning rules perform in an optimal fashion, with numerous oscillations that get smaller over time, but do not disappear. This is most likely due to the inability of the PRC test to develop a FOTD model that is accurate, and accounts for non-linear dynamics that emerge in the relationship between the CTAH motor frequency, the average temperature across CTAH, and the power input.

4.3.3 Relay Feedback Tuning

The Relay Feedback test was applied to the CTAH controller at normal steady-state conditions, with the power at 5 kW , the mass flow rate at 0.18 kg/s , and the initial CTAH outlet temperature at 80°C . The test was done with relay amplitudes of 2.0 Hz and 2.5 Hz . The test can be seen in Figure 29.

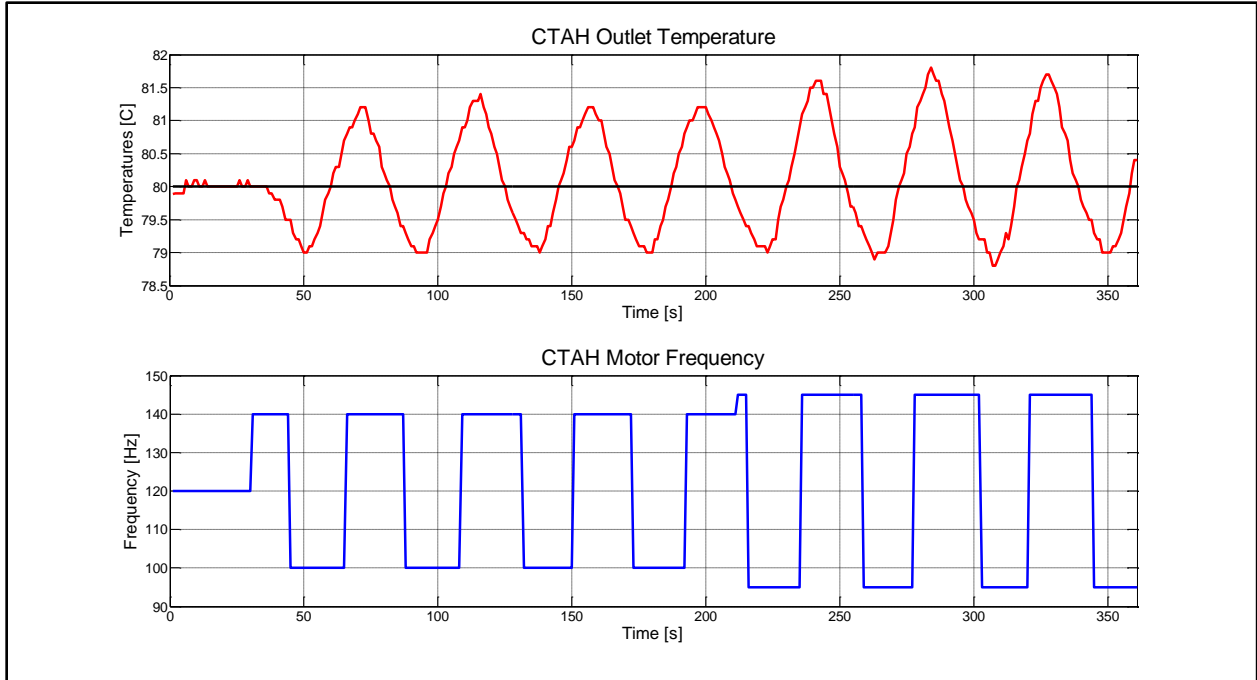


Figure 29. Relay feedback test for CTAH at normal, steady-state conditions and relay amplitudes of 2.0 and 2.5 Hz.

By analyzing the observed outlet temperature amplitude and the period of the temperature oscillation and the relay, it is found that the ultimate gain K_U is 23, and the ultimate period T_U is 42 s. Using these parameters with the ZN tuning rules yields optimal PID coefficients, which are listed in Table 4-4. The parameters were used to find the coefficients for a standard PID controller, a PID controller with no overshoot, and a PD controller.

Table 4-4. PID coefficients for CTAH control derived from the relay feedback test.

<i>Controller Type</i>	K_P	K_I	K_D
PID	14	0.67	74
PID (NO)	5	0.67	70
PD	18	—	95

The two PID controllers were tested for their ability to control the CTAH outlet temperature during start-up. The conditions were identical to the start-up process for testing the model-based PID controllers. The results of the start-up test can be seen in Figure 30.

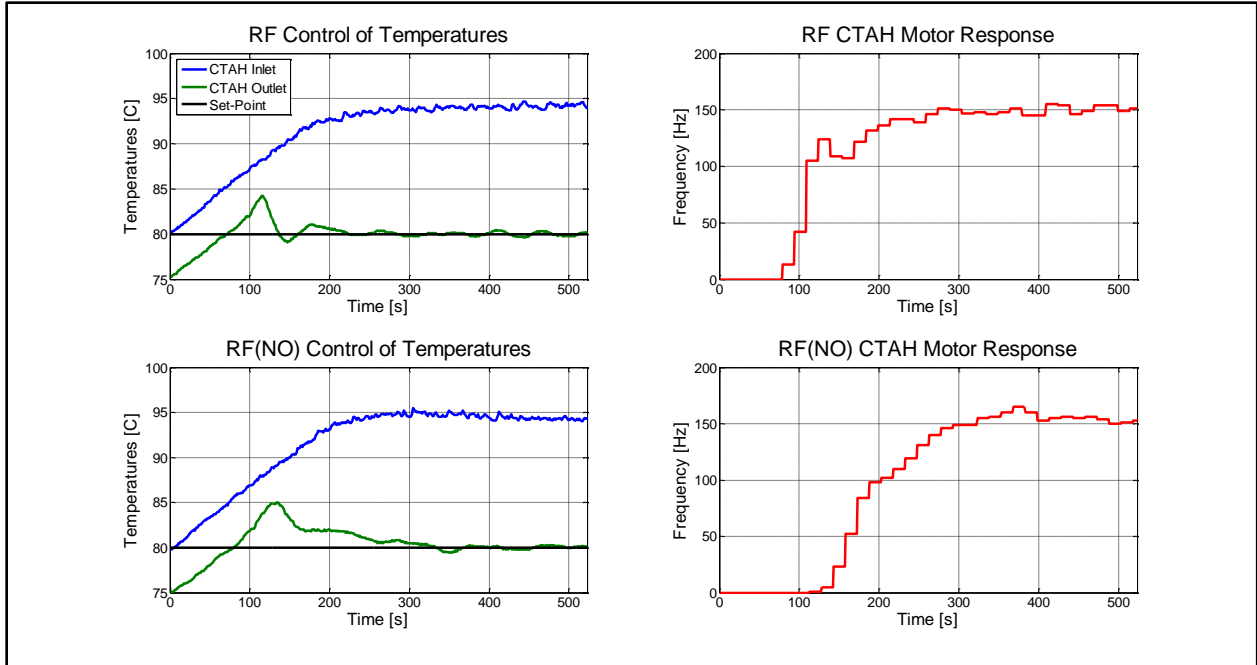


Figure 30. Comparison of a standard PID controller and a no-overshoot PID controller, derived from relay feedback testing, during CIET start-up.

Both controllers perform far better than the model-based controllers. The standard PID controller oscillates with an error less than 0.5°C , and converges to the set-point relatively quickly. The no-overshoot controller takes longer to converge, but oscillates with an error less than 0.3°C . Figure 31 shows a graph of the outlet temperature responses, overlaid on top of one another. Between the two tuning strategies, the standard PID controller is superior. It is possible that the no-overshoot PID controller would show improved performance if the integral wind-up threshold was increased; however, increasing this threshold would also likely exacerbate oscillations.

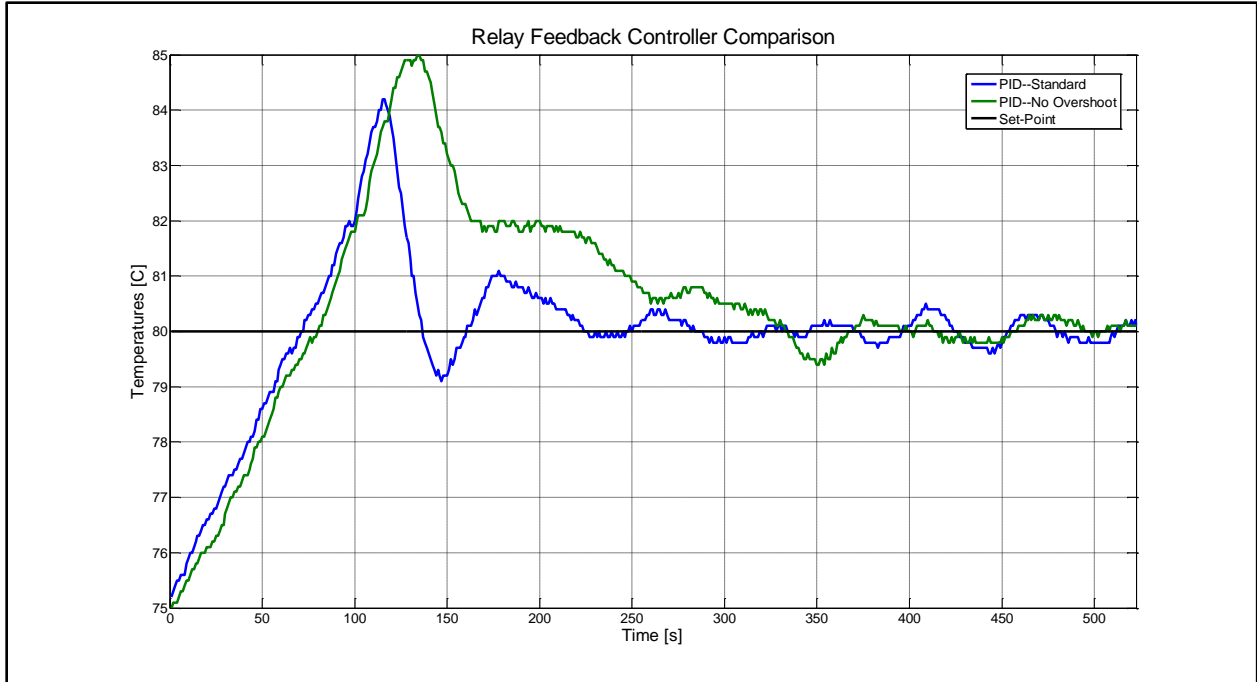


Figure 31. Comparison of the CTAH outlet temperature response when controlled by a standard PID controller and a no-overshoot PID controller.

4.3.4 Summary of Results and Recommendations

Of all the different controllers that were tested, the controllers that performed the best was the manually-tuned P controller, and the relay feedback tuned PID controller. Figure 32 shows an overlaid plot of the two controllers during a start-up process.

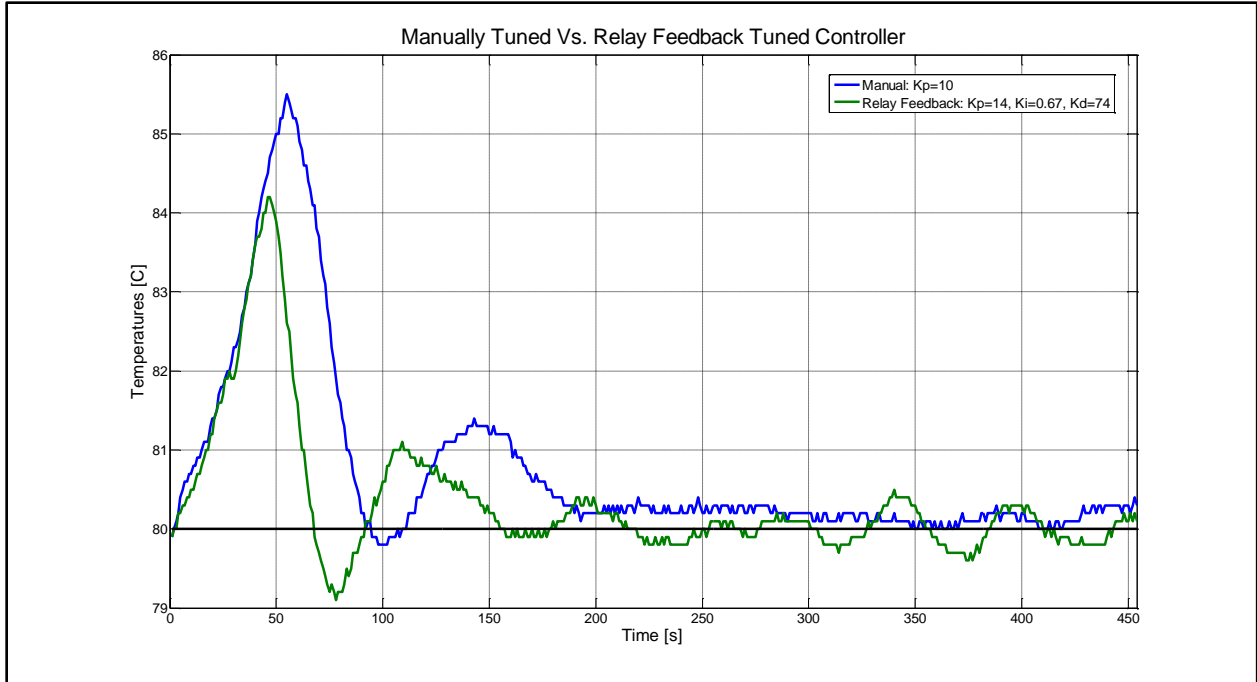


Figure 32. Comparison of a manually-tuned P controller and a relay feedback tuned PID controller during CIET start-up.

It is arguable that the manually tuned P controller exhibited better control performance than the relay feedback tuned PID controller. The convergence times are similar, and the outlet temperature is steadier under the P controller than under the PID controller; albeit with a steady-state error of around 0.3°C. However, for general tuning applications, the relay feedback tuning strategy is clearly more efficient in terms of labor.

4.4 TCHX

The primary goal of the TCHX controller is to control the output temperature of the heat exchanger. The TCHX is located on the DRACS loop, and is designed to extract at least 2 kW of energy out of the loop during normal, steady-state operation, with an outlet temperature set-point of 46°C.

For TCHX feedback control optimization, it was decided that Relay Feedback would be the optimal tuning strategy. This was based on the results of the CTAH feedback control optimization.

4.4.1 Relay Feedback Tuning

The Relay Feedback test was applied to the TCHX controller with the power at 2 kW, and the initial TCHX outlet temperature at 46°C. These are the expected normal operating conditions for the DRACS Loop. The test was done with relay amplitudes of 2.0, 3.0, and 1.0 Hz. The test can be seen in Figure 33.

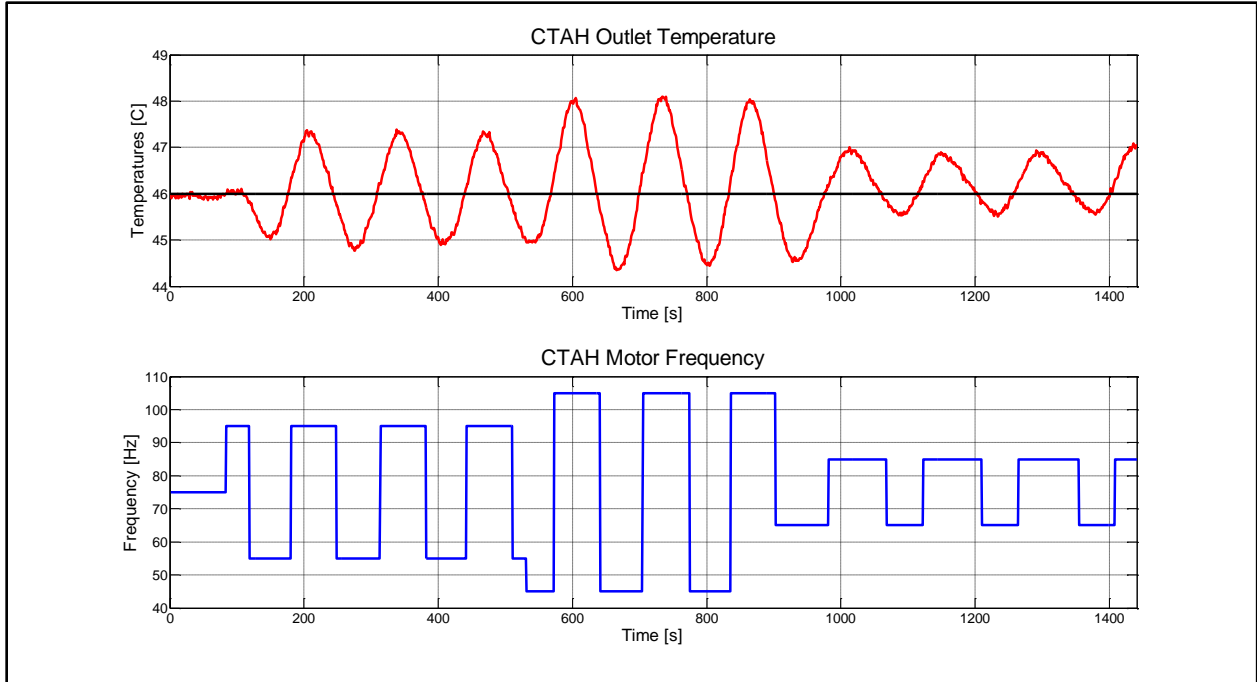


Figure 33. Relay feedback test for TCHX at power input at 2 kW with coupled natural circulation between the primary and DRACS loop, for relay amplitudes of 2.0, 3.0, and 1.0 Hz.

By analyzing the observed outlet temperature amplitude and the period of the temperature oscillation and the relay, it is found that the ultimate gain K_U is 21, and the ultimate period T_U is 132 s (these are averages from the results of the three relays). Using these parameters with the ZN tuning rules yields optimal PID coefficients, which are listed in Table 4-5. The parameters were used to find the coefficients for a standard PID controller, a PID controller with no overshoot, and a PD controller.

Table 4-5. PID coefficients for CTAH control derived from the relay feedback test.

<i>Controller Type</i>	K_P	K_I	K_D
PID	13	0.2	215
PID (NO)	4	0.2	176
PD	17	—	281

The two PID controllers were tested with the power at 2 kW, with the primary loop and the DRACS loop under conditions of coupled natural circulation. The initial conditions of the test were different, as there were difficulties in cooling the DRACS loop to a point where the same start-up scenario can be tested. However, because the disturbance source (the TCHX inlet temperature) was still the same for the majority of the test, the controller performances can still be compared. The plots of the test can be seen in Figure 34.

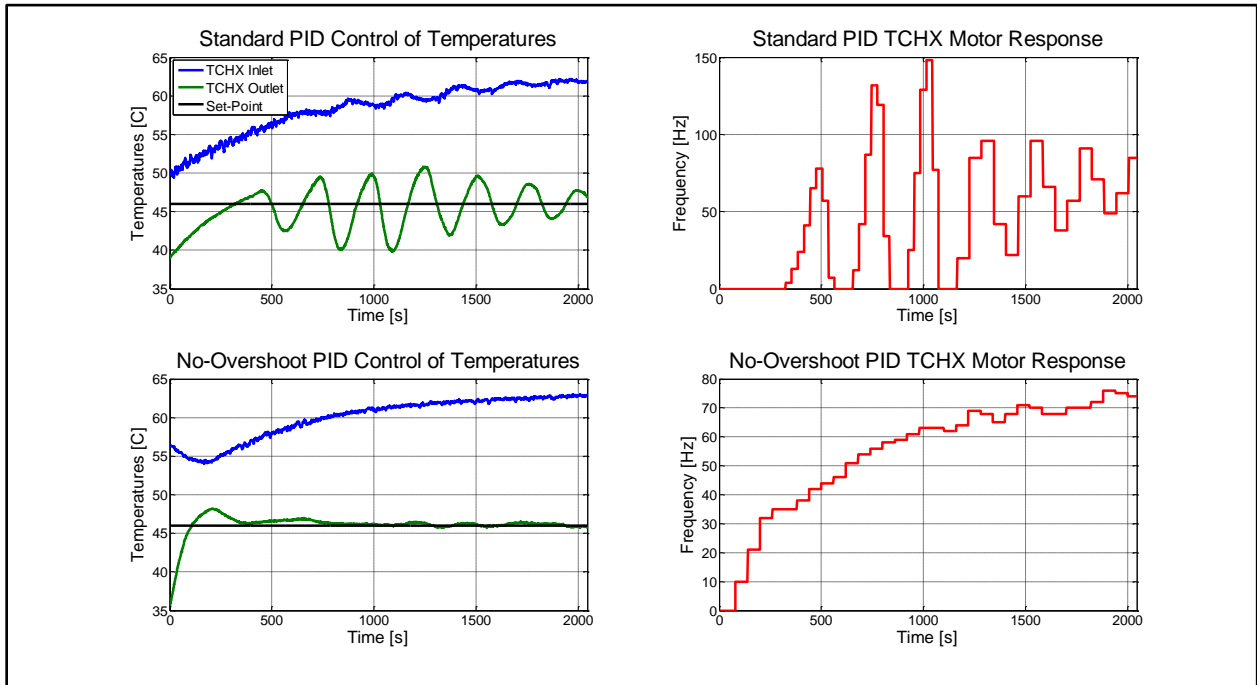


Figure 34. Comparison of a standard PID controller and a no-overshoot PID controller for the TCHX, derived from relay feedback testing.

The standard PID controller was tested with two different feedback timers: 30 s and 60 s. The timer was shifted to 60 s at approximately the 1100 second mark, at the bottom of the third minimum of the TCHX outlet temperature. The controller with a 30 s timer was unstable with increasing oscillation amplitude, while the controller with a 60 s timer was stable with a decreasing oscillation amplitude, but far too sluggish in convergence to be an effective controller.

The no-overshoot PID controller, with a feedback timer of 30 s, was effective at converging the TCHX outlet temperature with the set-point. Small oscillations, with an amplitude less than 0.4°C, persisted, but overall controller performance was acceptable for both convergence speed and stability.

5 LabVIEW Code Overview

This section reviews the LabVIEW code used to monitor and control CIET. The general code architecture is divided into different while loops, specific to instruments and controllers. There is a while loop for the data acquisition system that monitors thermocouple and flow meter values, another to control the VFDs for the pump and the heat exchangers, another to monitor and control the power supply, and so on. Each loop is generally self-contained; however in certain cases, it is necessary to pass data and commands between loops. Each loop also has its own independent timer on which the code is executed.

5.1 Instrumentation Data Acquisition

All thermocouples and flow meters are read through the SCXI set-up, which is processed via the LabVIEW DAQ Assistant. The DAQ Assistant outputs a data wire containing readings of all the channels attached to the SCXI set-up. This can be seen in Figure 35.

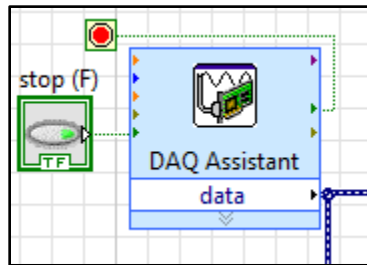


Figure 35. DAQ Assistant block.

The DAQ Assistant outputs signals in one single wire. In CIET's case, this means that all 51 signals (thermocouples and flowmeters) are combined into one dynamic data wire. In order to isolate specific signals, a splitter needs to be used that splits the single signal into 51 signals. The individual signals are then merged into packets that correspond to their physical location. The actual data contained in each signal output from the splitter is determined by the data order in the DAQ Assistant. Figure 36 shows the splitting and combining of the DAQ Assistant output data wire.

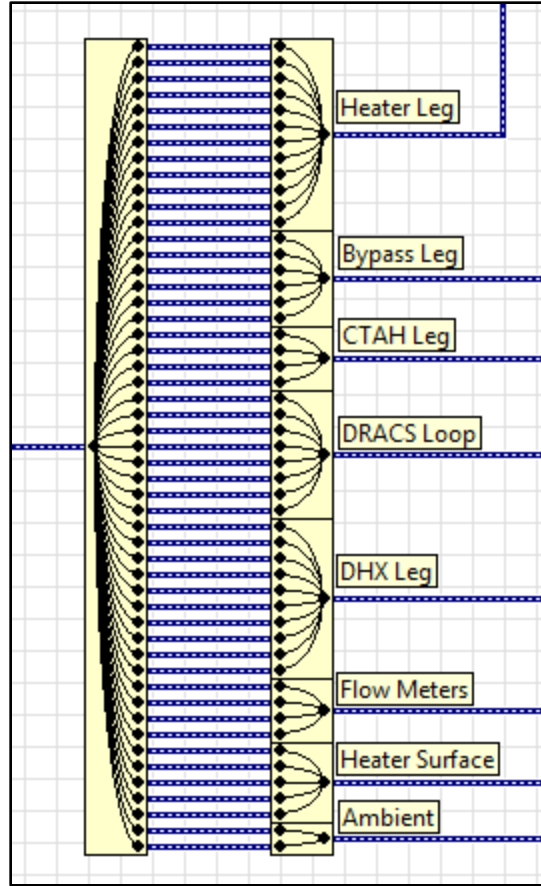


Figure 36. Splitting and combing the DAQ Assistant's data output wire.

5.1.1 Thermocouples

Each recombined data wire (packaged according to physical location in CIET) is then sent to a new splitter, which inputs the data into individual indicators. A data conversion function that converts to a “Double” is used to convert the dynamic data wire into a double data wire. For certain values, a sub-VI is used to average the wall and bulk thermocouple to find the average value. Figure 37 shows the final signal splitting, data conversion, and indicators for thermocouples in and around the heater.

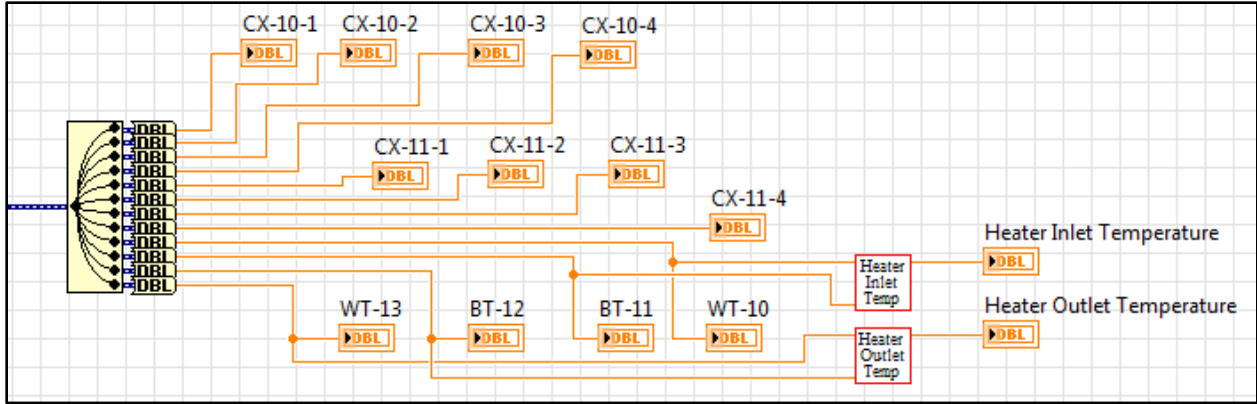


Figure 37. Final signal splitting and data conversion for heater thermocouples.

5.1.2 Flow Meters

There are four flow meters for CIET, one each in the CTAH, bypass, and the DHX branch of the primary loop, and one in the DRACS loop. The output from the DAQ Assistant is a current reading; this must be converted into a mass flow rate reading. There is one conversion factor for the DHX and the CTAH flow meters, and another for the Bypass and DRACS flow meters; these correspond to the fact that the DHX and CTAH branches are bi-directional, while the Bypass and DRACS branches are uni-directional. As such, there are two sub-VIs for current-to-mass-flow conversion, corresponding to the two different conversion factors. The flow meter signal splitting and conversions can be seen in Figure 38.

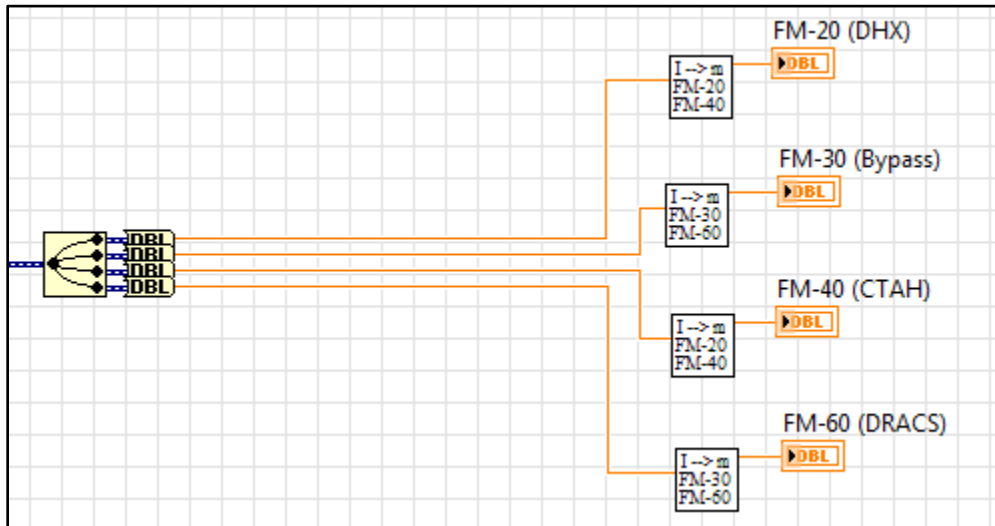


Figure 38. Final signal splitting, data conversion, and current-to-mass-flow conversion for flow meters.

5.1.3 Alarms

All temperatures are monitored for whether they exceed certain maximum values: this is 135°C for fluid temperatures, and 250°C for surface temperatures. These limits correspond to maximum temperature limits for Dowtherm A and the heater material. The sub-VI that monitors the extrema values of CIET, and its outputs, is shown in Figure 39.

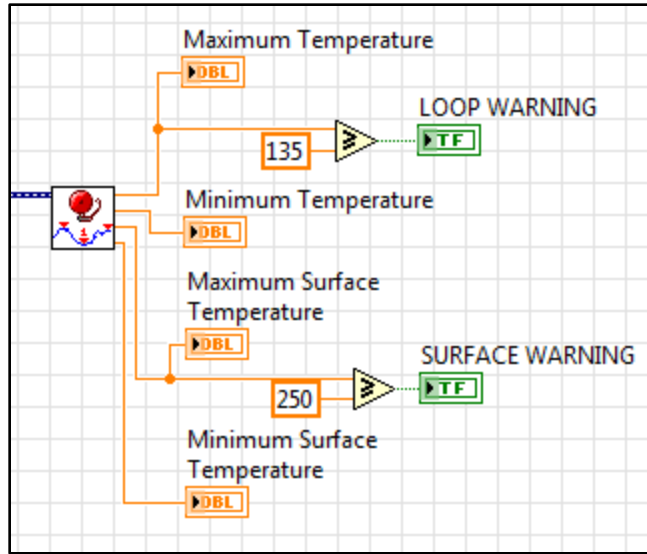


Figure 39. Temperature alarms for fluid and surface temperatures.

The alarm sub-VI code is similar to the main DAQ code; it takes in the DAQ Assistant data wire, and splits them into individual data wires. Inside the sub-VI, all the wires are fed into a build array function, which is then fed into a function that finds the minimum and maximum values of the array. These measured extrema are the outputs of the sub-VI. This can be seen in Figure 40.

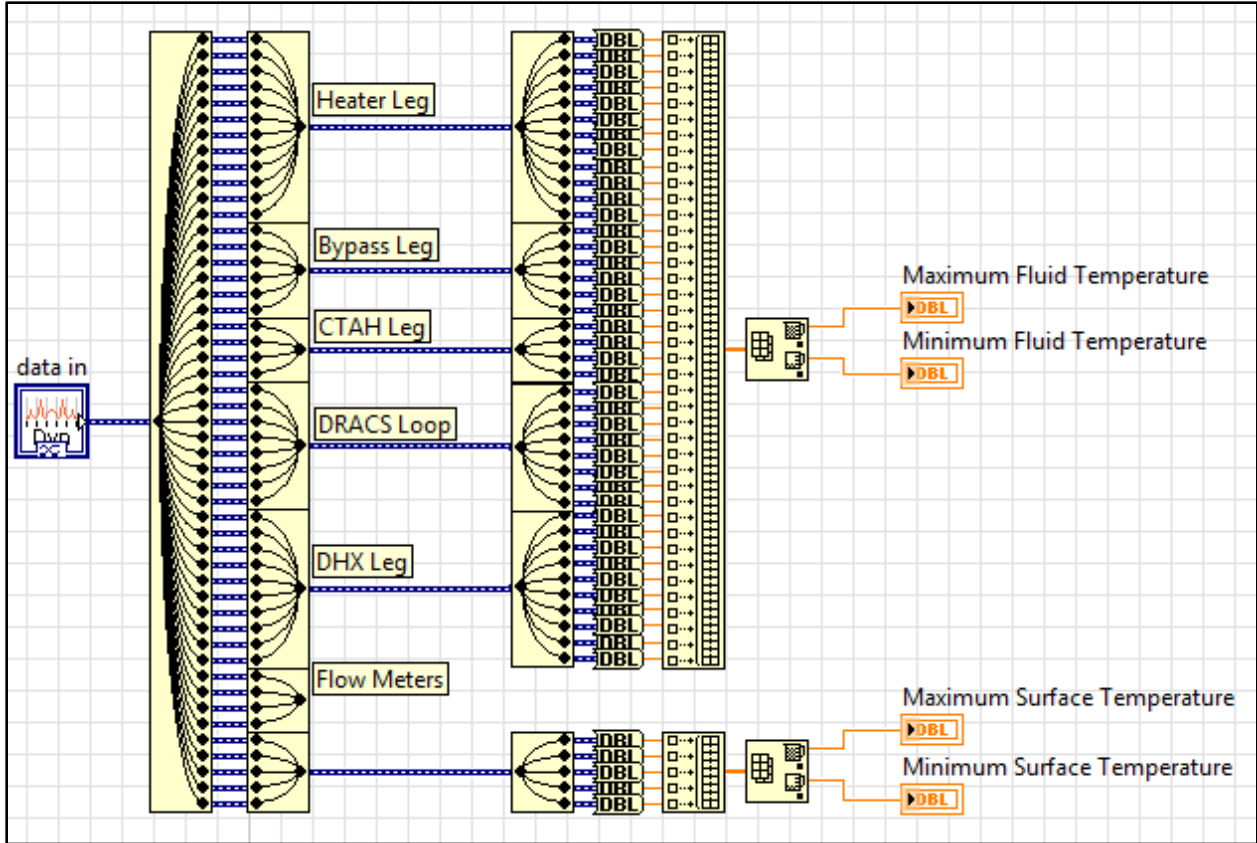


Figure 40. Alarm sub-VI code with array functions for finding the temperature extrema.

5.1.4 Notes on Extra Elements

For fully functional VIs, there will be some additional sections of code within the DAQ structure, such as error calculations for the feedback control algorithms and data bundling for graphs.

For error calculations, as shown in Figure 41 and Figure 42, the process variable is subtracted from the set-point (or vice versa, depending on the specific algorithm), and then processed through constraining functions and absolute value functions to ensure that the value is not out of range or noisy.

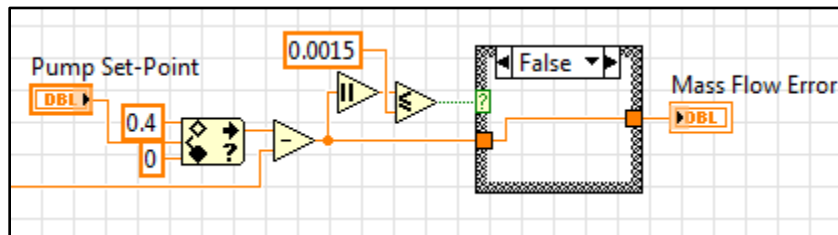


Figure 41. Error calculation for the Pump Mass Flow Rate.

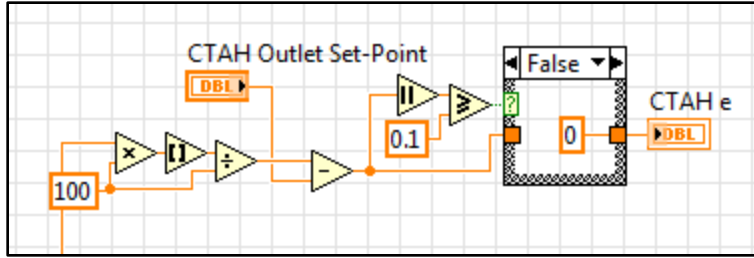


Figure 42. Error calculation for the CTAH Outlet Temperature.

Another important additional section of the DAQ loop is graphing. Graphing in LabVIEW is useful as the graphs can be exported into Excel sheets. Multiple data points can be bundled into a cluster using a “Bundle” node, as shown in Figure 43; bundling is useful for graphs as it allows multiple measurements to be overlaid on a single graph.

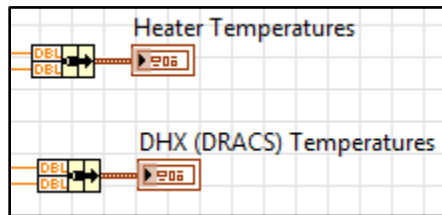


Figure 43. Example of bundling data measurements.

For data analysis, it is generally important to have the timing interval of recording the point on the graph be equal across data sets. Therefore, it is useful to have an independent loop with the graphing code so as to ensure consistency in the timing. Figure 44 shows a graphing loop that graphs data being sent from other loops.

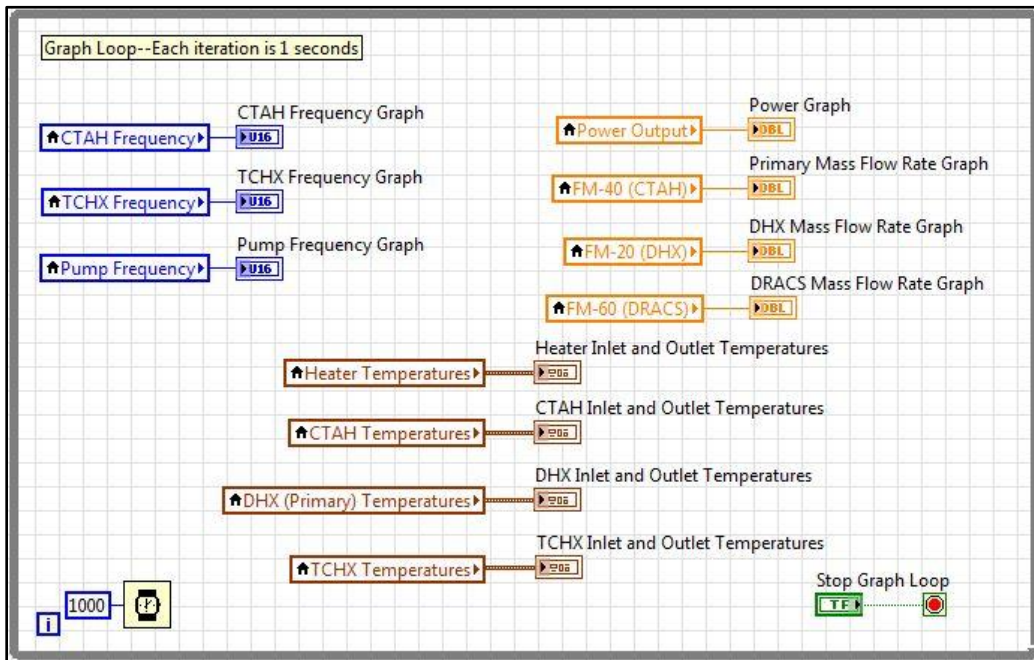


Figure 44. Graphing loop.

5.2 Variable Frequency Drive

The VFDs control the pump, the CTAH, and the TCHX by manipulating the frequency of their motors. There is one while loop controlling the input frequency and the operational state of the VFD, allowing the user to switch the VFDs on and off and manipulate the output frequency in real-time.

The front panel allows the user to toggle each VFD on and off, enter an automated parameter set-up process (necessary at the beginning of each test), manipulate each VFD's output frequency, and end the while loop. Figure 45 shows a version of the front panel.

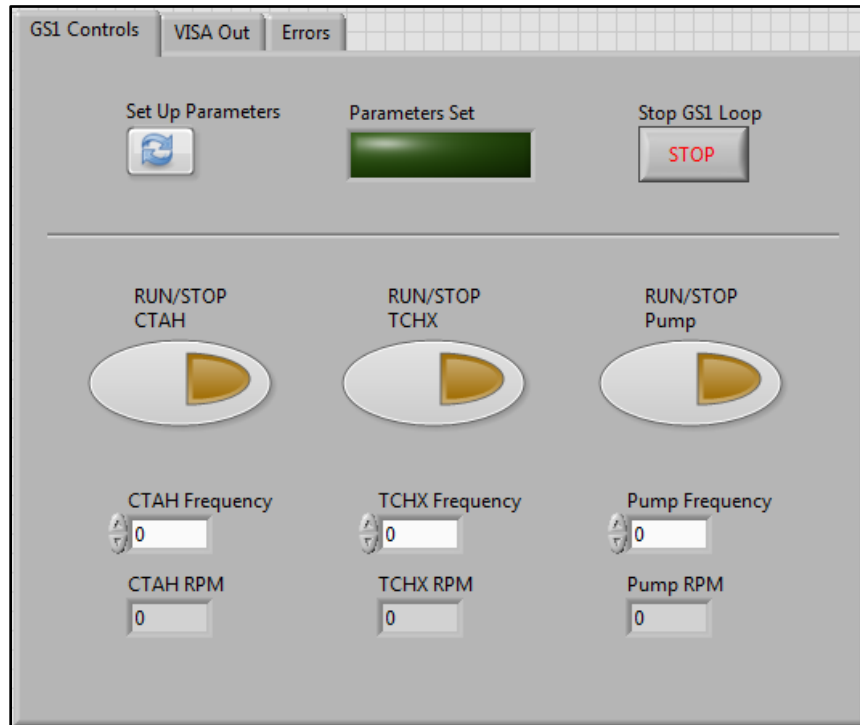


Figure 45. Section of a front panel for controlling the VFDs for the pump and fans.

5.2.1 Communication

The VFDs communicate to and from the computer using a serial port. LabVIEW communications through serial ports using VISA protocols to control instruments. The specific communication protocol used to control the VFDs is Modbus RTU. A Modbus sub-VI library developed by NI can be downloaded online.

The only sub-VI that is necessary is the “MB Serial Mastery Query”, set to “Write Single Register” mode. The critical inputs to this sub-VI are the serial parameters (communication mode and address), the serial port name (also known as the VISA resource target), the address, and the holding register. The address and holding register are specific to the parameter that the user wants to manipulate; the address specifies the parameter, and the holding register is the value that is to be written to this parameter. Figure 46 shows the code that writes commands to the CTAH VFD. There are two Modbus sub-VIs used for each VFD: one for controlling the frequency, and one for running and stopping the VFD.

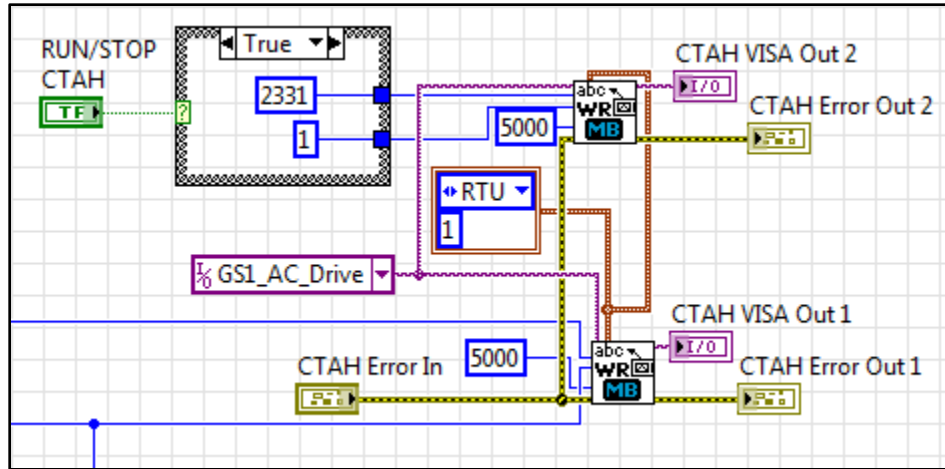


Figure 46. Inputs and outputs to the CTAH VFD's Modbus sub-VI.

5.2.2 Pre-Operation and Normal Operation

Prior to running the VFDs, certain parameters specific to the motors of the pump and the fans must be set. This is done via the “Set Up Parameters” button. This button controls a Boolean signal to a case structure. When the button is activated, the code within the case structure cycles through eight different Modbus addresses and holding registers, which correspond to eight different parameters. This cycling is accomplished with two components: a case structure with a feedback loop that counts from zero to eight, which sends each number to a sub-VI that contains the corresponding address and holding register. When the case structure is in its eighth state, it sets the “Set Up Parameters” button to off, switching the general case structure to normal manual operation. Figure 47 shows the counting code and the GS1 Set-Up sub-VI, and Figure 48 shows the sub-VI code.

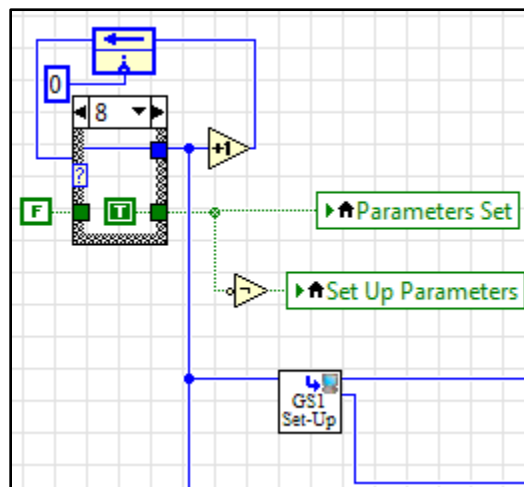


Figure 47. A counting algorithm to cycle the GS1 Set-Up sub-VI through the relevant sets of addresses and holding registers to prepare the VFDs for running.

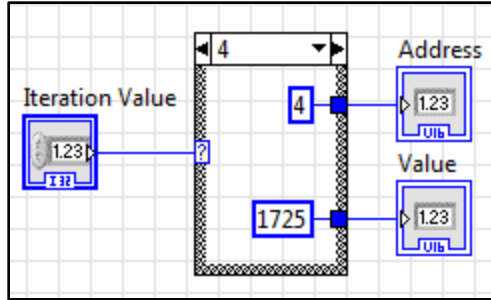


Figure 48. GS1 Set-Up sub-VI code for setting key parameters.

The normal operation mode of the case structure passes through frequency values (controllable from the front panel) to the frequency address. This can be seen in Figure 49.



Figure 49. Normal control mode for the CTAH VFD.

5.2.3 Emergency Stop Code for the Pump

The pump VFD has limits placed on its output frequency, as well as a monitor to prevent excessive mass flow rates in the primary loop, in order to prevent cavitation and resulting damage to the pump from occurring.

The limit is placed using a coercion function, that coerces the input value to be within the range—which in this case, is from 0 to 350. If a higher value is in the input, the output of the coercion function will be the maximum value. The monitor compares the measured CTAH mass flow rate with the maximum value of 0.4 kg/s; if this value is exceeded, then the case structure activates to shut off pump feedback and set the pump frequency to 50. This section of the code can be seen in Figure 50.

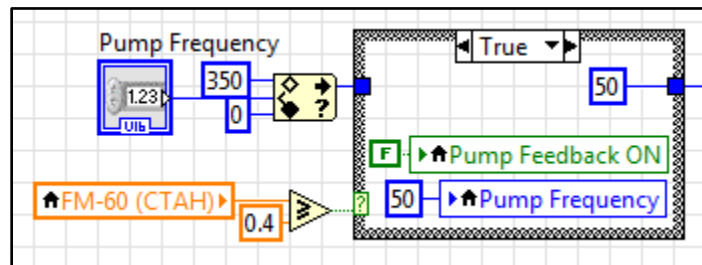


Figure 50. Pump VFD frequency coercion code and primary loop mass flow rate monitor.

5.3 Power Supply Base

CIET uses two 10kW power supplies, in series, to provide power to the resistive heater. Both power supplies use VISA-based serial communication to communicate to and from the computer. The simplest way to control the power supplies is to set the desired voltage limit. For CIET, a feedback algorithm based on resistivity measurement is used to enable the user to directly set the desired power output. The physical and mathematical basis for this algorithm is explained in Section 4.1. Figure 51 shows the power supply front panel control, where the user can control whether the power supply is supplying power, and what the desired power input to CIET is.

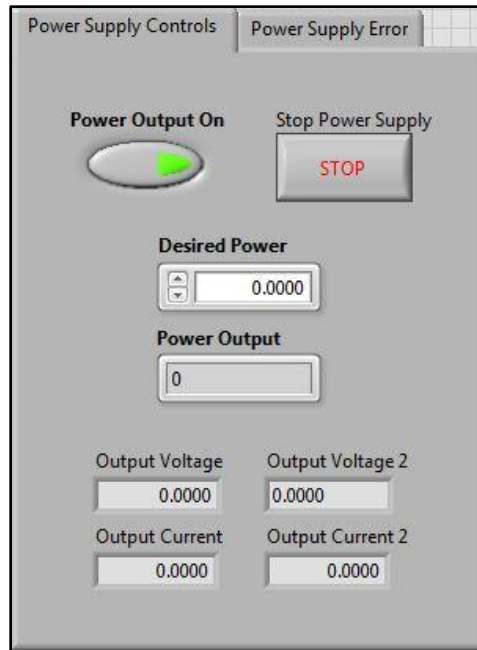


Figure 51. Front panel for power supply control.

5.3.1 Communication and Initialization

Lambda-TDK offers sub-VIs that host most of the required communication programming that is necessary for remote control of the power supplies. Figure 52 shows the section of the code that initializes the power supplies with the correct serial port, addresses, baud rate, and control mode. The addresses and baud rate selected must match the addresses and baud rate set in the power supplies. This section is outside of the main while loop, and thus executes only once, at the very beginning of each test. The control mode specifies whether the power supply is measuring the voltage with the local sensor (at the output of the power supply) or the remote sensor (at the load). CIET uses remote sensing, with a baud rate of 9600.

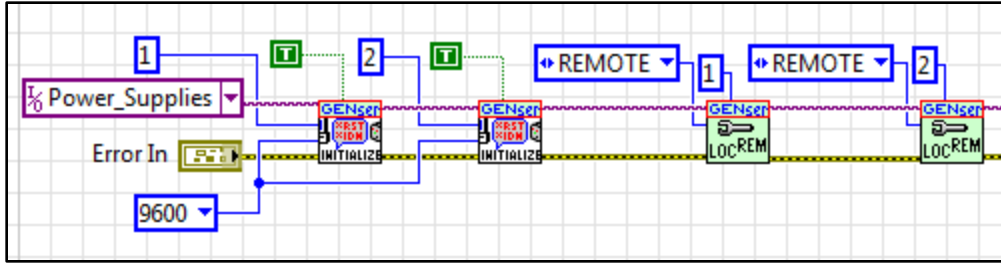


Figure 52. Initialization code for the power supplies.

5.3.2 Voltage/Current Control Code

The core section of the power supply control code executes different functions one at a time, in series. The primary sections of this code, consisting of seven sub-VIs connected in series, can be seen in Figure 53. First, there is a 20 ms delay, which allows signals to properly get communicated and processed. Second, the voltage limit is set, which is determined by the feedback code based on the desired power and the measured resistivity. Third, the current limit is set (which is constant at 1000 A). Fourth, the power supply is set on or off, depending on the Boolean control. Fifth, there is another 20 ms delay to allow for proper signal communication. Sixth, the output voltage is measured. Seventh, the output current is measured. For this set of sub-VI execution, the specific address is set at the voltage limit sub-VI; all subsequent sub-VIs will communicate to this address unless a new address is specified.

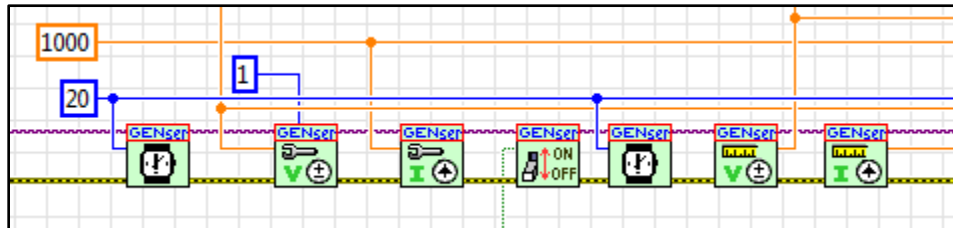


Figure 53. Series of sub-VIs for controlling and monitoring one power supply.

The voltage limit input to the “Set Voltage Limit” control sub-VI is calculated based on the “Desired Power” value that is set by the user, and is passed through a series of calculations, which is seen in Figure 54. This value is constrained by a case structure that determines whether CIET temperatures are within safe limits (if not, the power supply is automatically turned off), and whether the desired power is between 0-10kW (if the desired power is set higher, it is automatically constrained to be 10kW). This value is then multiplied by the calculated resistance value, which comes from the shift register (seen as the arrow at the left edge, on the frame of the while loop). After another couple of calculations, in accordance with Ohm’s Law, the voltage limit corresponding to the desired power and current resistance value is calculated.

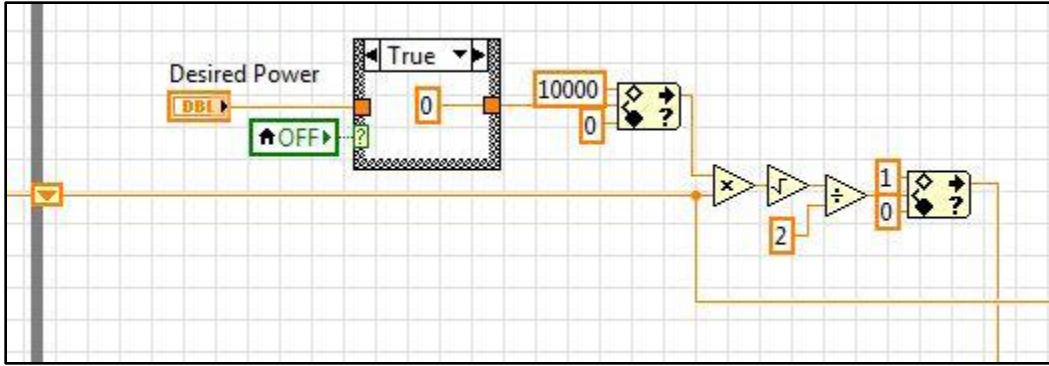


Figure 54. Section of power control code that converts the Desired Power into the voltage limit.

The resistance value is calculated via Ohm’s Law, and the shift register transports this value to the next loop in order to set the voltage limit.

One potential problem arises from the fact that sometimes it takes a few loop iterations for the voltage output of a power supply to reach the actual limit. This can cause distortions and instabilities in the resistance calculation because it is miscalculating based on an old value of the voltage. In order to give the voltage output time to increase/decrease to the voltage limit, a case structure is used that only allows a new resistance value to be passed on if the voltage output of both the power supplies are within 0.02 V. Another potential problem is that because of delays in the output voltage and output current readings representing the actual values, the calculated resistance spikes extremely high (toward infinity). In order to avoid this, the resistance value is constrained between physically possible values. These strategies are packed into one section of the power supply control code, as seen in Figure 55.

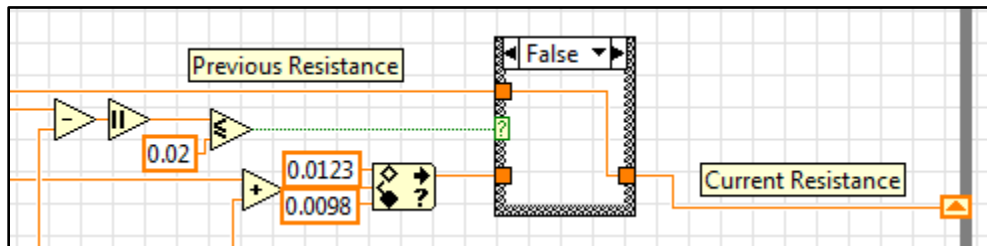


Figure 55. Processing the resistance calculation prior to transferring it to the next loop iteration.

5.4 Feedback Control Algorithm

The pump, CTAH, and TCHX use variations of PID feedback controllers in order to control the output frequency of their respective VFDs. The general structure of the LabVIEW PID code was developed such that the user can toggle the PID controller on and off, and thus smoothly transition between manual and feedback control.

The general structure of the PID code has three layers: a while loop, which is inside a case structure, which is inside a primary while loop. The primary while loop monitors whether the frequency is controlled manually or through feedback, looping on a one-second timer. The case structure contains the actual code for the feedback control; when feedback control is off (and

manual control is on), the case structure is empty. When feedback control is on, the inner while loop activates, and executes the feedback control algorithm.

The feedback controller algorithm takes in an initialized value for the frequency, which is recorded as the value right before the feedback control was turned on. Initialization is necessary to create a smooth transition from manual to feedback control, because the default initial value for the shift register is zero, which would create a discontinuity and possible instabilities during the switch.

Depending on the kind of feedback controller (proportional, proportional-integral, etc.), the algorithm may contain different summing and multiplication codes, and different inputs from other loops. Figure 56 shows a proportional controller code used for controlling the pump; the code executes every two seconds, and the input to the “Pump Frequency” is the sum of the previous iteration’s “Pump Frequency” value and the product of 700 (the proportional coefficient) and the “Mass Flow Error”, in accordance with the proportional control algorithm described in Section 4.2.

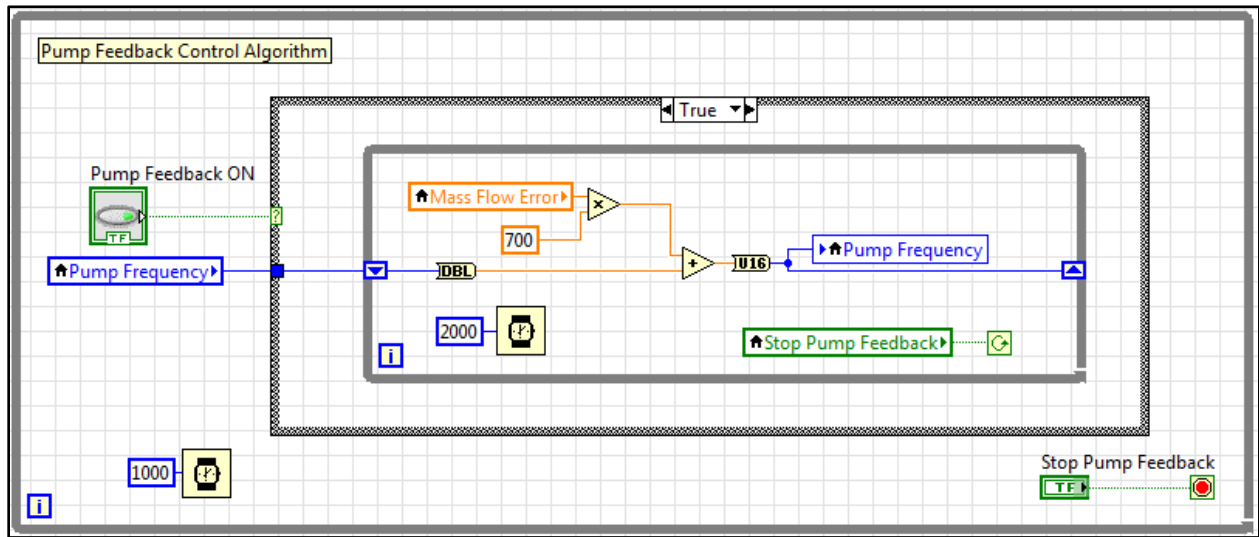


Figure 56. Proportional controller for the pump.

The most complex feedback controller used is the PID controller, like the one used to control CTAH. This requires additional loops to calculate the integral and derivative terms. The integral loop sums the error over a certain period of time, which is very useful when there is a steady-state error that is large enough to cause distortions in the system, but too small for the proportional action to actuate. The derivative loop calculates the rate of change in the process value, which is very useful to anticipate and counter-act rapid changes in the process and avoid excessive overshoot or undershoot.

Figure 57 shows the CTAH’s PID controller; it is similar to the pump’s P-controller, but has two more summing terms before the “CTAH Frequency” is changed.

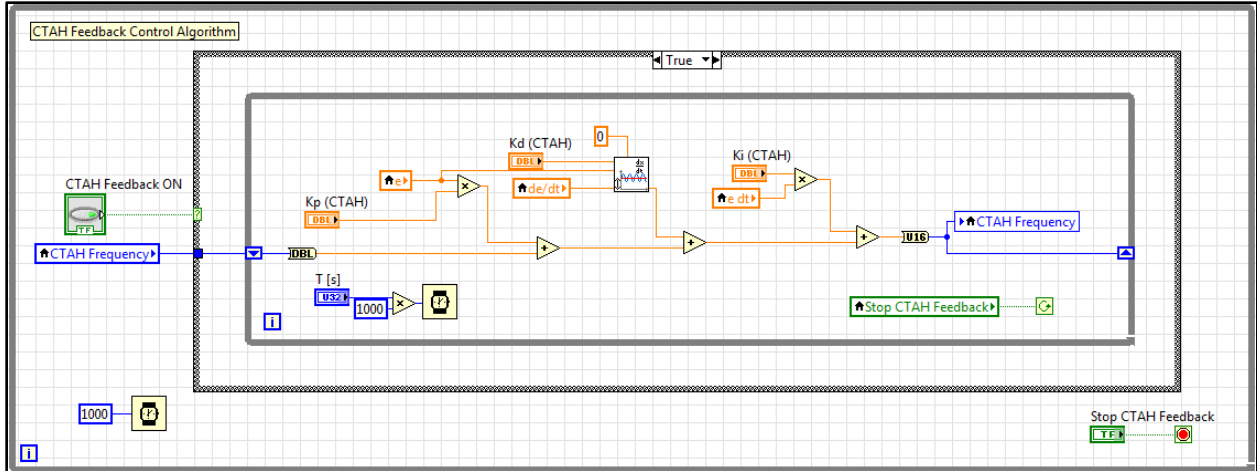


Figure 57. The CTAH PID feedback control algorithm.

The integrator takes in the error as an input, and processes it through a rounding function so that only two significant figures remain; this is done by multiplying by 100, rounding, and then dividing by 100.

The error is then processed through a block of code that functions as an anti-windup algorithm, which only passes an error value if the error is greater than 0.5°C. Anti-windup is a strategy to prevent integral action from creating large changes in the process output and possible instabilities during set-point changes. In general, integral action should not be used when the process value is far away from the set-point, since the main point of integral action is to act on small, steady-state errors that proportional action cannot deal with.

The error is then passed to a block of code that acts as a reset algorithm. A case structure is linked to whether or not the current loop iteration is a multiple of 15; if it is, the error is reset to zero, and if it isn't, the error is passed to a shift register after adding to the previous iteration's accumulated error. The integrator loop can be seen in Figure 58.

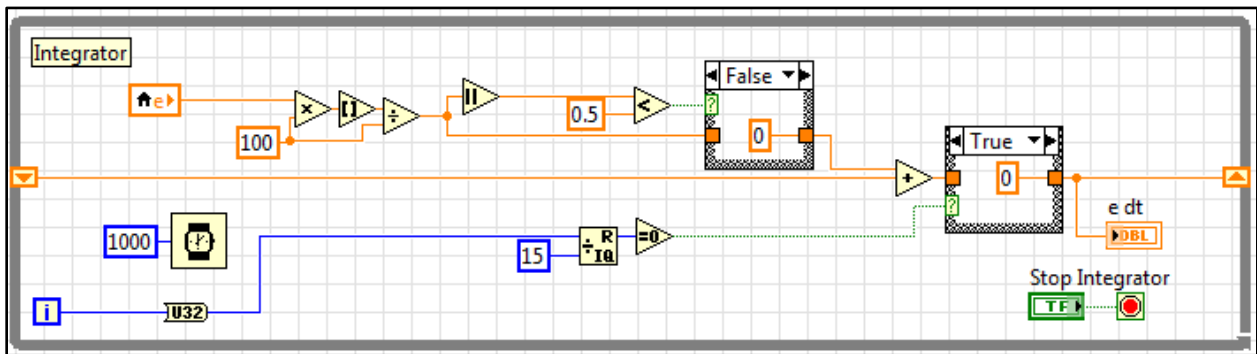


Figure 58. Integrator loop.

The differentiator processes the outlet temperature rather than the error, so as to avoid step-changes in the error due to set-point changes. The temperature value is passed through a rounding function like in the integrator. This value is then subtracted from the previous loop iteration's measured temperature value, and then converted into a value with units of degrees

Celsius per second. The value of the rate of temperature change is then sent through a coercion function to ensure that the value makes physical sense. The differentiator loop can be seen in Figure 59.

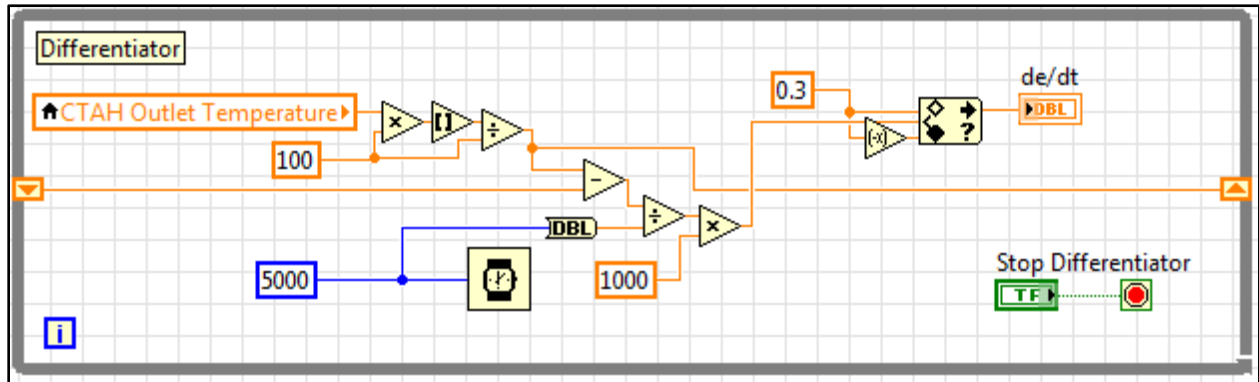


Figure 59. Differentiator loop.

5.5 Relay Feedback

Relay Feedback is a PID tuning method, described in Section 3.3, which involves creating a square wave input to the process, whose period is based on the process response time. The user sets the relay amplitude and the base value (the “zero” of the square wave). For the LabVIEW code, the user must also set a “Noise Gate” in order to ensure that noise around the base value doesn’t disrupt the square wave’s amplitude transitions, and a “Relay Timer” that sets how often LabVIEW polls data coming from sensors. The Relay Feedback Loop for the CTAH is shown in Figure 60.

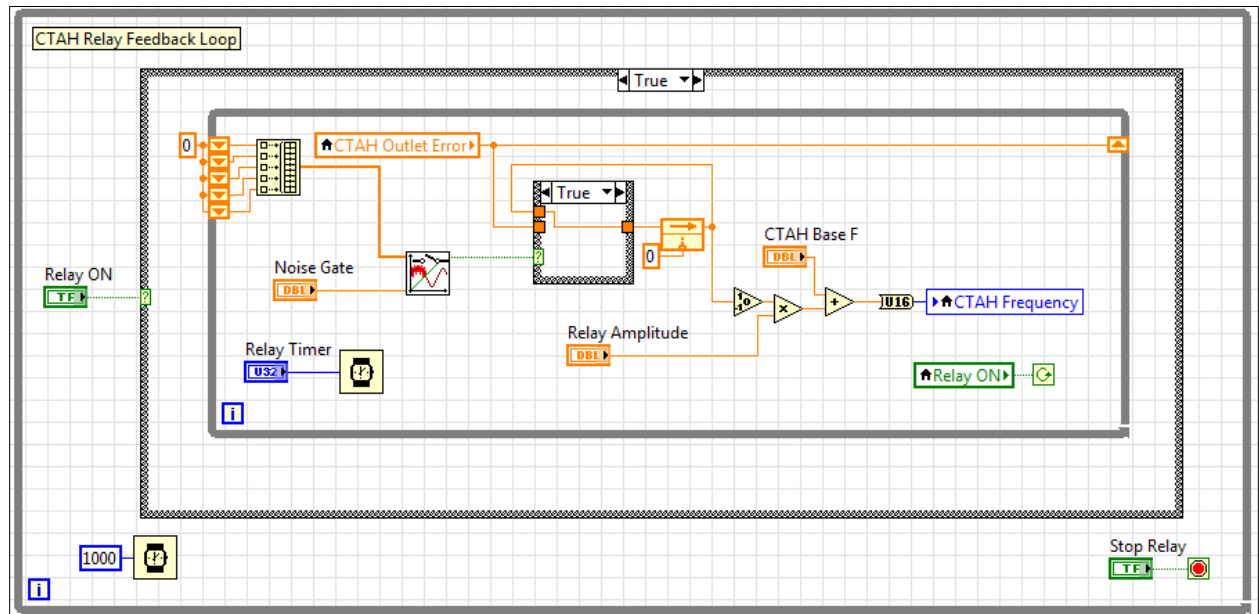


Figure 60. Relay Feedback Loop for tuning the CTAH.

The Relay Feedback Loop for the CTAH acts on the “CTAH Outlet Error”, which is calculated in the same way as the PID loops discussed in Section 5.4. The “CTAH Outlet Error” should correspond to the “CTAH Base F”, such that the error is zero for the base frequency under the initial conditions of CIET prior to the relay being activated. In other words, relay feedback tuning should be from steady-state conditions, which the user must manually control.

One aspect of the code to note is the “Noise Gate”, which ensures that noise from the thermocouples around the zero-degree point does not result in noise in the relay feedback (since the relay is tied with the sign of the error). The noise is “gated” using code in a Sub-VI, shown in Figure 61.

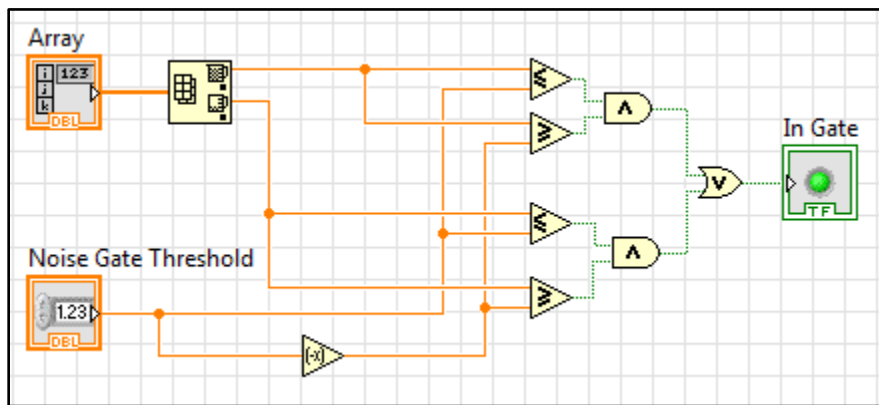


Figure 61. Noise gate code for optimal relay feedback performance.

The “Noise Gate” analyzes the array of five previous temperatures and compares them with the “Noise Gate Threshold”, which creates a buffer zone around the zero-degree mark. Only when the five consecutive temperature measurements are outside the buffer zone is the relay allowed to act on the measured sign of the error.

Initialization of the relay feedback is done manually, by entering in a “CTAH Frequency” that is the upper value of the square wave (“CTAH Base F” + “Relay Amplitude”). This will start decreasing the CTAH temperature, and thus drive the “CTAH Outlet Temperature” to be negative. After the frequency is changed, the Boolean control “Relay ON” should be switched on, turning the control of the frequency over to the relay feedback logic. Once the relay is activated, the negative error should trigger the “CTAH Frequency” to be switched to its high value. At this point, the relay and the “CTAH Outlet Temperature” should stabilize with relatively consistent amplitudes and periods. After three to five periods, there should be enough data to use the analysis described in Section 3.3 to derive the optimal gain coefficients for a PID controller.

6 Summary and Conclusions

CIET's sub-systems were integrated with instrumentation and controllers, incorporated into a central LabVIEW system, and optimized for stability and user control. As of May 2015, CIET was fully operational, with its controllers demonstrating satisfactory and reliable performance.

The two power supplies were successful at using a resistance-based feedback controller for power input control, and indicates that this strategy can be deployed for other experimental systems using electrical resistive power supplies. The flow rate in the primary loop was effectively controlled by the pump VFD with a simple P controller that was tuned using predictions from known physical parameters and correlations. A variety of different control strategies were used for tuning the PID controller on the CTAH, ranging from trial-and-error manual tuning to model construction-based tuning. It was concluded that model construction was both labor-intensive as well as ineffective at controlling the non-linear processes that underpin heat transfer, and that relay feedback tuning rules were the most effective. Relay feedback was subsequently used for tuning the TCHX, and it was found that the no-overshoot relay feedback tuning rules were the most effective controller.

For the optimization of the actuation frequency for all the controllers, no real theory was tested; tuning relied entirely on manual, user based tuning. As a general rule of thumb, it can be concluded that the actuation frequency must have some relationship with the time lag between a change in the manipulated variable and a corresponding change in the controlled variable.

LabVIEW proved to be an effective and versatile platform in which to integrate hardware and develop and optimize control algorithms. The built-in front panels were also effective at allowing for intuitive user control of CIET.

With an effective control strategy in place, CIET is set to accelerate its validation of FHR processes and dynamics, and begin engaging in more complex phenomena. The experiences and lessons learned during the development and optimization of CIET's instrumentation and controllers can also apply to other heat transfer and fluid dynamic systems dealing with similar sub-systems and physical phenomena.

7 References

- Andreadas, Charalampos. *Technical Description of the “Mark 1” Pebble-Bed Fluoride-Salt-Cooled High-Temperature Reactor (PB-FHR) Power Plant*. UCB-TH-14-002. 2014.
- Anthony S. McCormack and Keith R. Godfrey, “Rule-Based Autotuning Based on Frequency Domain Identification”, *IEEE Transactions on Control Systems Technology*, Vol 6, No 1, 1998.
- D.I. Wilson. *Relay-based PID Tuning*. Automation and Control. 2005.
- GS1 Series Drives User Manual*. Automation Direct. 2nd Edition. July, 2011.
- Ziegler, J.G. and Nichols, N.B. *Optimum Settings for Automatic Controllers*. Transactions of the American Society of Mechanical Engineers. No. 64. 1942. pp759-768
- Astrom, K.J. and Hagglund T. *Automatic Tuning of Simple Regulators with Specifications on Phase and Amplitude Margins*. Automatica. Vol. 20, No. 5. 1984. pp645-651.
- Sung, Su Whan, Lee Jietae, and Lee, In-Beum. *Process Identification and PID Control*. IEEE Press, John Wiley and Sons (Asia) Pte Ltd. 2009.
- Thermocouples: Introduction to Temperature Measurement*. Omega. 2015.
<http://www.omega.com/prodinfo/thermocouples.html>
- Technical Manual for Genesys 10kW/15kW Programmable DC Power Supplies*. TDK-Lambda Americas Inc. 2008.
- Zweibaum, Nicholas. *SITRANS FC430 Coriolis Flowmeters Technical Sheet*. CIET-MES-TS-002-01. Thermal Hydraulics Group. 2014.